Chapter 2
Rainfall and Floods

Abstract There are different types of rainfall depending on elevation, temperature, or pressure differences that generated by composition of various meteorological factors such as light, moderate, or extreme rainfall occurrences with or without flood consequences. In arid regions, elevation (orographic) and temperature (convective) differences may cause to floods, but in humid regions, pressure difference (frontal) rainfalls are the major factors. In order to calculate various rainfall characteristics such as the intensity recording, raingauge records are necessary, but with accurate measurements. Different sources of measurement errors are explained in the text with their correctional actions in the field and office. Various areal average rainfall calculation methodologies, especially innovative percentage-weighted methodology, are presented in comparison with the classical and about 100-year-old Thiessen approach. New concepts such as the dimensionless intensity–duration curves are explained, and their application to annual maximum rainfall amounts is presented with actual data processing. The importance of the intensity–duration–frequency curves is explained with the concepts of different risk levels. The significance of probable maximum rainfall and its connection with probable maximum flood calculation is presented through the applications to a set of drainage basins from the western part of the Kingdom of Saudi Arabia. Efficiency factor is defined the first time in the text for distinction of the climate change impact on the rainfall occurrences in the region.

Keywords Areal average · Efficiency factor · Error · Hyetograph
Dimensionless intensity · Intensity–duration curve rainfall · Probable maximum rainfall · Probable maximum flood

2.1 General

Floods are consequences of a set of rainfall premises among which are the rainfall type, regime, amount, duration, frequency, and intensity. Rainfall records are available at a set of meteorology stations, and measurements are recorded by the

Z. Şen, *Flood Modeling, Prediction, and Mitigation*,
https://doi.org/10.1007/978-3-319-52356-9_2

meteorology service of each country. In general, there are two types of rainfall records; the first one is total rainfall measurements during the whole period of the storm rainfall event, which includes the duration and the total rainfall height. A sequential collection of total measurements includes more than one storm rainfall in the form of a time series, which is very important for description of wet and dry period features as well as extreme values that may cause floods or droughts. The next type is the record of rainfall amounts during each storm rainfall in a cumulative manner, which gives a basis for rainfall intensity, duration, and frequency (IDF) calculations. Such records are important for determining the rainfall intensity for the design of many engineering structures based on the return period and risk level (Chaps. 5 and 7).

The most important meteorological event in the lower atmosphere (troposphere) is the precipitation that is the source of all water resources in the world. It is the fall of any solid (snow, hail) and fluid (rain) drops from the cloud bottom to the earth surface. After the reach of precipitation on the earth surface, not the meteorological principles, but the hydrological laws govern the surface and subsurface flows. The very first task is to measure the temporal and spatial variations of the precipitation by a set of convenient measurement instruments, which are referred to as the raingauges. The measurements from a raingauge are the records that provide temporal behavior of the precipitation event at the meteorology station location and around its nearby surrounding. Preliminary assessments of the records provide the initial interpretation opportunities to reach at information about the rainfall height, time durations (hour, week, month, season, and year), and areal extent. Further, refined calculations provide severity, magnitude, duration, intensity, and frequency of dangerous events such as floods and droughts. As for the water resources, rainfall and the snowmelt are the two major contributions. In order to plan and manage the entire water resources, one should try and obtain basic information, interpretation, and conclusions about the areal and temporal characteristics of the rainfall. Such activities are significant in water resources planning, management, irrigation, and agricultural activities. The types, intensities, frequencies, areal coverages, and averages are very important statistical quantities for the design of flood magnitude, risk, and occurrences. In Chap. 6, the probabilistic and statistical evaluation of the rainfall and consequent flood evaluation are presented for future predictions.

The chief characteristic of a heavy rainfall event as flash flooding and such an event (in any region) can be described as a natural hazard that causes major floods and severe destruction, often resulting in loss of lives and damage to property. It is, therefore, necessary to understand and be able to follow the evolution of a heavy rainfall event at the event scale. Such an assessment provides considerably beneficial information to scientists, in general, and to the administrative authorities of a region, in particular. Sudden and rapid occurrences of flash floods in natural channels present technical challenge to scientific modelers and decision-making administrations. They are linked to intensive thunderstorms, and they are also highly localized. Trapp et al. (2007) mentioned that apart from producing dangerous lightning and torrential rainfall, such thunderstorms are responsible for

high-impact weather, including destructive surface wind, hail storms, and/or tornadoes.

In any water study, the rainfall is the basic variable and it is expressed as the amount of rainfall over unit area during unit time or snowmelt water depth equivalent per area. For instance, when monthly rainfall is said to be 35 mm, it means that over 1 m^2, the rainfall depth is 35 mm and the following points must be taken into consideration in the same context:

1. It is the amount of rainfall that falls onto the surface from the clouds prior to any loss of evaporation, depression, and infiltration; hence, it is also the amount of global rainfall on the ground surface.
2. The rainfall has three important units as area—m^2; depth—m; and time duration, which may be day, month, or year. It is not enough to say that the rainfall amount is 15 mm, because its duration as hour, day, etc., must be specified as total, average, low, extreme, or any other value.

Effective rainfall is obtained after the subtraction of evaporation and infiltration from the gross rainfall amount in this chapter. If rain falls on a frozen or completely impervious or saturated soil surfaces, then infiltration cannot take place, so that once the initial interception and depression storage are satisfied, the remaining rainfall contributes to runoff and to possible flood. The amount of the surface moisture in the soil influences the infiltration capacity.

Frequency of inundation depends on the climate, the material that makes up the banks of the stream, the channel slope, and drainage basin surface features (Chap. 3). Where substantial rainfall occurs in a particular season each year, or where the annual flood is derived principally from snowmelt, the flood plain may be inundated frequently every year, even along large streams with very small channel slopes. In regions without extended periods of below-freezing temperatures, floods usually occur in the highest precipitation season. The regions, where most floods are the result of snowmelt, are accompanied often by rainfall during spring or early summer seasons.

Rainfall is the main source of the world's freshwater supplies. Nature and characteristics of a storm rainfall help to predict its effect on runoff, infiltration, groundwater recharge, evapotranspiration, and water yield calculations. The volume of flow rate for storage or conveyance by the drainage system can be related mathematically to the rainfall storm features such as intensity, duration, and frequency. The main interest is to know the likelihood of occurrence (probability) of an event with a specified intensity and duration, which are inversely related.

This chapter is concerned with the description, definition, quantification, and estimation of different rainfall characteristic amounts and some applications, especially in arid lands.

2.2 Causative Reasons for Rainfall Occurrence

The travel of precipitation from the cloud base to the earth surface is of concern to meteorologists. They are concerned with the generation of clouds as a result of evaporation and transpiration, the rising moist air (water vapor), and their cooling and condensation to form the clouds. For precipitation, the presence of clouds is necessary, but not sufficient, because each cloud does not yield precipitation. The water particles and ice crystals, especially in the upper layer within the cloud, move randomly in various directions at small scales. Since they are very small, they can escape the gravitational effects. Even today, physical reasons for precipitation generation within the clouds are not understood completely and there is vague information about it. Microscale irregular movements do not provide a common base for the precipitation generation mechanism fully scientifically. For precipitation, the cooling, condensation, and drop growth stages must be completed successively. In general, for the precipitation generation there are four stages:

1. Existence of enough water vapor in the air as the source of clouds,
2. Drop in water vapor temperature below dew point for condensation,
3. Water drops' cooling leading to ice piece generation,
4. Growth of drops and pieces that reach to a scale that cannot escape the gravitation force, and hence, precipitation starts from the cloud base and reaches to the measurement instruments on the earth surface.

2.2.1 Water Vapor

Evaporation and transpiration release to the air invisible water vapor together with small water drops and microscopic solid pieces, which make up the humidity in the air. The humid air rises and originates the clouds, but at lower elevations, it appears as fog. Water phases appear in different diameters, and according to their scale, they can be grouped into different classes. Water vapors in the form of gases have diameters around 10^{-4} micron; cloud drops have 5–100 micron diameter; 100–500 micron diameters are for ice crystals; and precipitation drops have diameters in the range 500–5000 micron. Snow and hail pieces have bigger diameters. Inside the cloud, these various diameter pieces are in a mixture and they move randomly. In open and clear air (without cloud), the water vapor pressure is small, but in cloudy weather precipitable water vapor increases between the earth surface and the cloud base. Air saturation causes dew point to increase with increasing temperature. In fact, the content of precipitable water vapor is higher in summer seasons than winter periods. In general, the amount of precipitable water at a location is dependent on the air thickness, latitude, distance, and elevation from the sea level, general circulations in the atmosphere and on the specific meteorological features of the location.

2.2.2 Cooling

Initially, for precipitation occurrence in the troposphere, sufficient amount of water vapor must exist. Water vapor is necessary for precipitation, but it is not sufficient. For cooling, according to thermodynamic rules, the air must expand, which is the main reason why clouds come into existence at certain heights from the earth surface. In other words, if water vapor laden air rises due to any cause, then it expands and cools. For a given temperature, there is a certain amount of air content. The air temperature varies according to air saturation ratio. As the temperature increases, the water content of the air also increases. Reduction in the air temperature causes incapability of air to accept more water vapor. The air cools down to a certain temperature according to the water vapor amount in the air and then onward cannot accept additional water vapor; i.e., the air is in the form of saturation. After this stage, further reduction in the temperature causes water vapor condensation. During the contact of saturated air with cold air, respectively, dew, ice, and fog start to appear.

During condensation moist air releases, heat, and hence, becomes cooler. The major factor that causes air to cool down is due to heat exchange, i.e., adiabatic state and the pressure fall. The rising and cooling effects of the air cause troposphere to be in a dynamic state continuously. The following factors individually and collectively cause to dynamism in the troposphere.

(a) Convergence lifts: The air movement from different directions toward a point is referred to as the convergence (Fig. 2.1). In this manner, at low elevations, the air converges and forcefully rises and such a vertical movements cause air to cool down.

Among the events that cause to convergence are the momentum difference between longitude and latitude, air movement to low-pressure centers from high-pressure centers, topographic hindrances, and divergence event at high elevations.

Air convergence events occur especially at tropical zone frontal areas, at low-pressure valleys, convergence of different valleys to direct the wind movement to a certain location, and tropical cyclones.

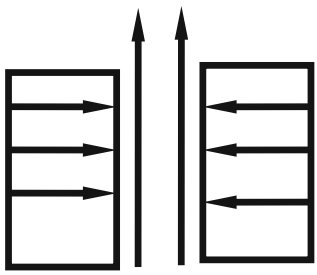

Fig. 2.1 Convergence event

(b) Frontal lifts: Confrontation of cold and warm air masses generates slopes similar to topographic features (Fig. 2.2).

In case of warm air over the cold one, frontal surfaces are generated from 1/100 to 1/300 slopes. On the contrary, in cold fronts, the cold air has steeper slopes (1/25 to 1/300). Over the sloppy plane, the air is forced to rise. In case of cold fronts, the slope is higher, and consequently, the warm air rises to higher elevations, and hence, short duration, but intensive rainfalls occur.

(c) Orographic lifts: As in Fig. 2.3, the air that is loaded with water vapor forcefully raises over the hill slope surfaces with wind effect. Ascending air starts to cool down, and logically, the speed of ascend is dependent on the hill slope and the speed of the wind.

The vertical speed reduces with the elevation and as has been documented by various researchers that even 50% reduction appears at 1000 m. Mountain hill slopes are continuous and steeper than the frontal slopes. In these regions, the air raises speedily and, therefore, results in longer duration rainfalls. This is the main reason why mountainous regions receive abundant and long duration rainfalls.

(d) Turbulence lifts: This lifting operation occurs in small and large scales continuously in a sophisticated manner (Fig. 2.4).

The small-scale turbulences happen at the boundary layers as a result of physical topographic hindrances. This causes water vapor to rise forcefully and generates thin layers of clouds at low elevations. Bigger scale turbulences are due to air dynamics at higher elevations along with the conventional movements. This mechanism may even cause water vapor to cross over the troposphere.

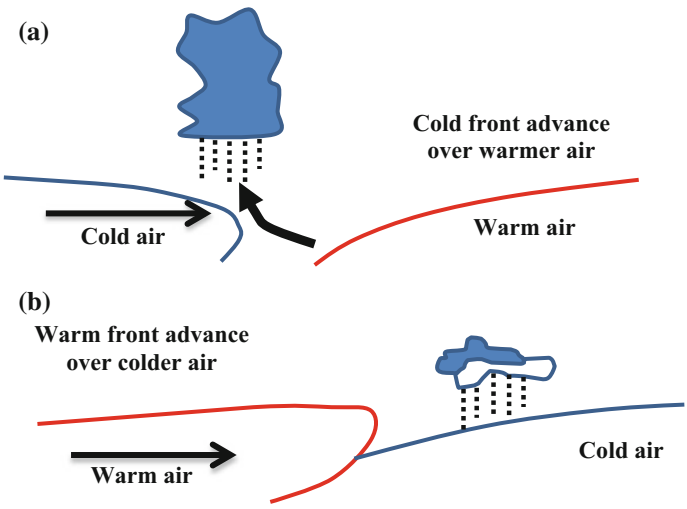

Fig. 2.2 Fronts–(**a**) cold, (**b**) hot

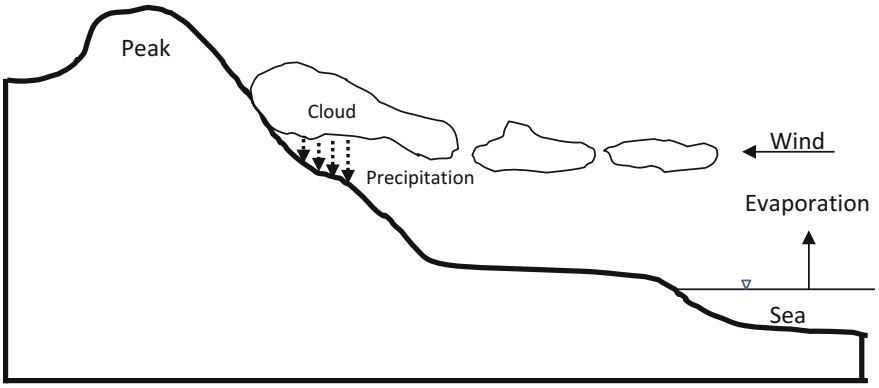

Fig. 2.3 Orographic lift

Fig. 2.4 Turbulence lifting

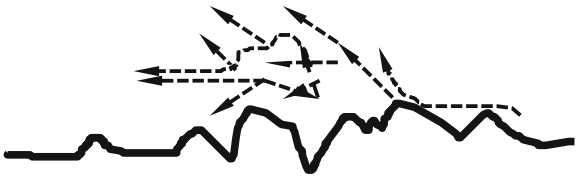

All the aforementioned lifting mechanisms come into existence after the instability of stable air due to various effects. In the imbalance of air, the following factors play a significant role:

(a) Cooling from bottom: In summer seasons, frequently observed phenomenon is the air cooling from below. As a result of this vertical cumulus, cumulonimbus clouds are formed (Fig. 2.5). Cumulus clouds are rather puffy and look like cotton heaps. Its base is almost flat and at about 1000 m above the earth surface. Its top is like a round tower, and it grows upwardly.

Similarly, as a result of upper latitude air mass movements toward the lower latitudes, the air becomes into contact with relatively warmer surface temperatures, the cooling is from the bottom, and hence, the air balance is disturbed.

(b) Upper cooling: If the water vapor in the atmosphere, especially in the upper troposphere, is dry and little, but the lower air layer is relatively moister, then the solar radiation can penetrate dry air easily, and hence, the lower moist air layer is heated from above. As a result, there are variations in the vertical temperature profile and the stability of air is disturbed, which causes thunderstorm and lightning prior to rainfall occurrences.

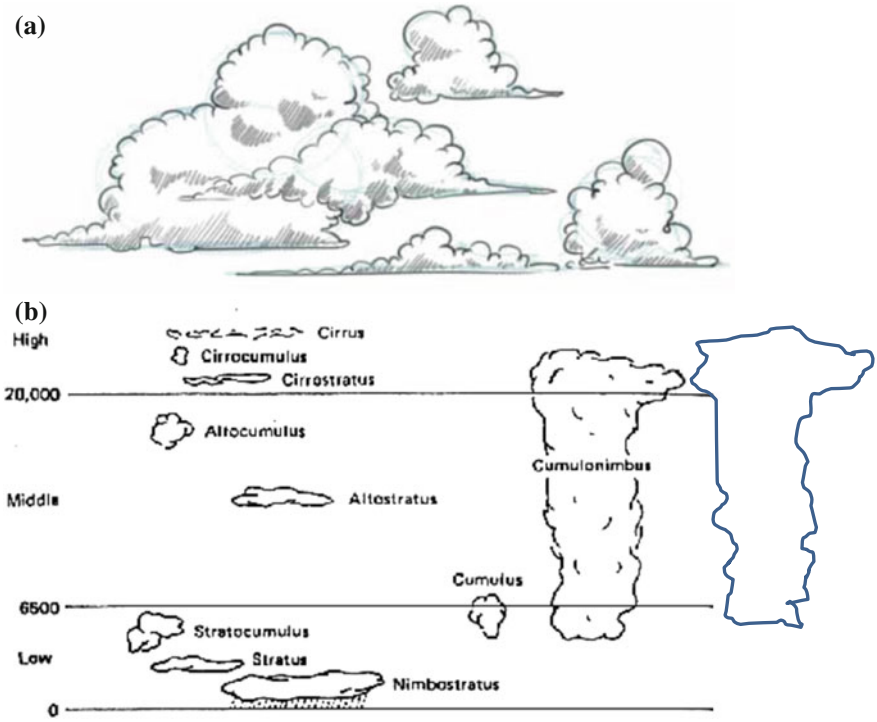

Fig. 2.5 Clouds, (**a**) cumulus, (**b**) cumulonimbus

(c) Conditional instability: If an air layer is between the dry and saturated vertical temperature differences, instability occurs as a result of lifting. If there are topographic and frontal effective risings, the air cools down to condensation-level dry vertical temperature difference, but after that, the cooling is due to saturation of vertical temperature difference. As a result, movement starts freely, because of the vertical temperature difference convectionally.
(d) Air layer lift: Below the air layer very moist and above it dry and relatively less moist air existence cause to air instability.

2.2.3 Condensation

With the cooling of air, the internal water vapor condenses and forms very small water drops. For this process, condensation kernels are necessary. These kernels can be dust and pollution particles that have risen from the earth's surface due to various reasons, and also, they can be salt pieces from the seas and oceans as well

as the pieces that are born from the meteors outside the troposphere. The cooling is possible with temperature decrease, but it is not sufficient for condensation, if the kernel particles are not available. It is for this reason that those who search for the artificial rainfall generation (cloud seeding) throw dust and very small pieces of sand into the clouds. In the absence of such particles, even if the air is 100% saturated, the condensation process does not take place. In the atmosphere, frequently there are chlorides and sulfur oxides for condensation and their diameters are smaller than 10 micron.

After the above-mentioned processes, prior to the precipitation generation, various water particles move randomly inside the cloud toward the upper layer. Under general synoptically valid conditions, the speed of this movement is very small (35 m/hour), but in the cumulus type of clouds, it is very high (70 km/hour). It is not possible that each saturated air always condenses. The air with its movement toward the ceiling of the cloud may be overcooled, and therefore, oversaturation takes place. Entrance of condensation kernels into such air causes precipitation.

2.3 Precipitation Types

It is already understood that for precipitation fall from the bottom of the clouds, three components should coexist. These are water vapor, solid condensation kernels, and a dynamic cooling mechanism. Depending on the type of the dynamic mechanism, three precipitation types occur. Each mechanism is dependent on some physical precipitation causative factors.

2.3.1 Elevation Difference (Orographic)

As already explained in Sect. 2.2.2, the clouds that are loaded with moist air and solid condensation kernels are carried horizontally due to the winds. When these clouds hit high mountains, they rise forcefully and become cooler leading to heavy drops as a result of further cooling and the gravitational force causes water drops to leave the clouds (Fig. 2.6). This is the type of orographic precipitation. The areal extent of such precipitation events is rather small.

2.3.2 Temperature Difference (Convective)

The meaning of the word “convective” is vertical movement in the troposphere, and they occur as a result of temperature difference, because hot air rises. Especially at flat surfaces of the earth, heating of low albedo parts gives rise to moisture and the

Fig. 2.6 Orographic precipitation

solid particle movements toward higher elevations, and hence, cooling process takes place (Fig. 2.7). By time the water drops grow further and again, the gravitational force causes precipitation. Such precipitation types are rather local and cover small areas. For instance, occurrence of rainfall in some part of the cities, but no precipitation in the adjacent quarters, is due to this type of cooling mechanism.

This rainfall type occurs most often in the tropical belt of the world, and the Hadley general circulation starts from the equator due to extra heating, because of the perpendicular solar radiation fall on the earth's surface. Most of the rainfall occurrences in desert areas are of this type. They are very common, especially in summer seasons, and occur frequently over areas that are surrounded by mountains. In summer, the air becomes moister due to evaporation, transpiration, and evapotranspiration from the soil. This causes hot air rises over the earth's surface, rising air expands and cools down, and finally, at a certain elevation, precipitation occurs

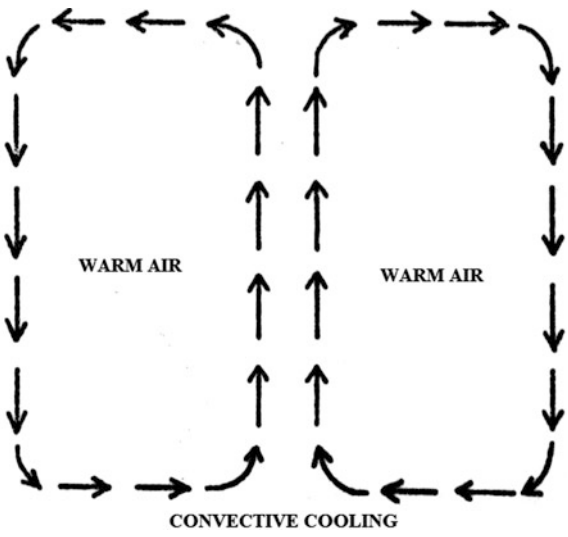

Fig. 2.7 Convective precipitation

following the condensation. The soil includes moisture in the autumn and summer seasons, and these also trigger convective rainfall occurrences. In particular, after abundant rainfalls during winter season, the soil ends up with saturation, which is the major factor of convective rainfall occurrences in summer seasons. These rainfall types are coupled with thunder, lighting, and even with occasional hail incidences.

2.3.3 Pressure Difference (Frontal)

Establishment of low- and high-pressure centers at various locations over the earth generates pressure differences, which move hot and cold air masses toward each other, and their hit gives rise to frontal precipitation. The moist air condenses due to the cold air effect, and hence, rainfall takes place. Compared with the two other types, the frontal rainfalls cover long distances and extensive areal coverages. They take place along the hot and cold frontals as in Fig. 2.8. In this manner, air masses laden with moist air in some country may end up with frontal rainfalls in some other country. The duration of these rainfalls is very long compared with the two other types and may continue for days and even for months. The rainfall amount has no comparison with other types, and it is very big.

2.4 Rainfall Measurement

Rainfall-related events such as floods and droughts can be evaluated provided that an effective monitoring system is available at different locations. Accurate and reliable observations and measurements are fundamental factors that provide sound bases for various engineering calculations in order to make dependable predictions. The raingauges must be located conveniently at local climate representative locations in a region. In general, the selection of convenient measurement locations should take into consideration the following points.

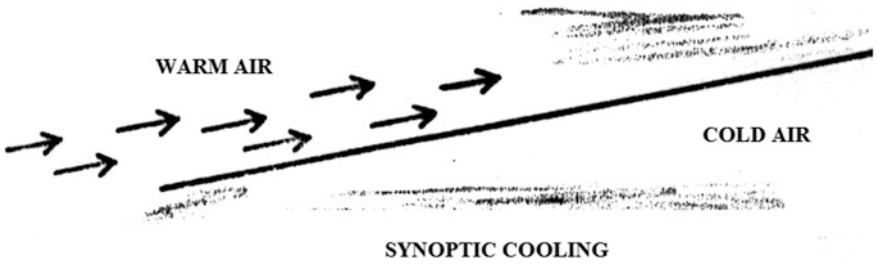

Fig. 2.8 Frontal precipitation

1. Easy transportation, flat or slightly sloppy areas are preferable.
2. The raingauge location must be extensive without ditches and hills.
3. The nearest hindrance to the gauge location should be at least three times the height of the object.
4. The gauge locations must be away from materials such as dust and chemical pollution sources and sinks, highways, railways, construction areas.
5. The peripheral boundary of the gauge must be such that neither animal nor human can get near to the gauge itself.

Information about the rainfall regime of any region can be obtained through the past records numerically and from local people linguistically. For this purpose, the rainfall records must be kept at regular time intervals and also at a set of locations for future prediction and planning activities. The amount of rainfall at any location is dependent on the surface features (geomorphology), persistent wind direction, and other meteorological factors including temperature, solar irradiation, humidity. Possible errors that may appear in raingauges are as follows:

(a) Defects from the gauge itself,
(b) The gauge locations might not be determined properly, and the instrument rim should be at about 30 cm above the ground,
(c) In case of insufficient raingauges or nonexistence of monitoring network.

2.4.1 Non-recording Raingauges

Instruments that record rainfall amounts at regular time instances or in a continuous manner are raingauges. In general, they have three major parts: cylindrical rainwater collection storage tank; funnel that gives way for rainwater to enter the storage smoothly and more specifically that hinders evaporation losses during non-rainy periods, and a graduated staff for rainfall amount measurement (Fig. 2.9).

These instruments provide rainfall heights at the gauge location. The more uniform is the rainfall distribution over a region, the less is the number of needed

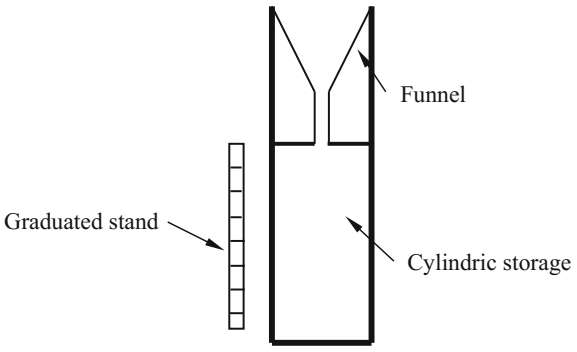

Fig. 2.9 Non-recording raingauge parts

Table 2.1 Minimum density of raingauge network

Region property	Minimum	Tolerable
Flat regions of temperate, Mediterranean, and tropical zones	600–900 km^2	900–3000 km^2
Mountainous areas of temperate, Mediterranean, and tropical zones	100–250 km^2	250–1000 km^2
Arid zones	1500–10,000 km^2	
For small islands	25 km^2	

10% of these gauges should be of recording type to enable the determination of rainfall intensity

gauges. This means that in rough terrain and mountainous areas, comparatively more dense raingauges must be located. In general, one raingauge is enough per 800–1000 km^2. The World Meteorological Organization (WMO) has given certain norms for the minimum network density as in Table 2.1.

2.4.2 Recording Raingauges

These are three types depending on mechanical, hydraulic, and electronic functions. In the mechanical type, a standard tank that stores rainwater is located on a balance, and as the water accumulates, the balance reflects the records on a chart located on the surface of a continuously and timely rotating cylinder. According to the revolution speed of the cylinder, daily or weekly accumulative rainfall records can be traced. In Fig. 2.10, hydraulically working recording raingauge is given.

The recording raingauges provide continuous records over long-time durations, and in a single chart, there may be more than one rainfall event. The chart records rainfall amounts continuously without any gap during the rainfall event. The records are in the form of continuously increasing curve forms as shown in Fig. 2.11.

This chart provides much information about an individual rainfall event at different time instances during the rainfall duration. The following points are some of the useful information deductions from such charts:

(a) The number of rainfall events at the station location can be counted easily from the chart. For instance, in Fig. 2.11 there are four complete rainfall events as R_A, R_B, R_C, and R_D.
(b) One can know the beginning, t_b, and ending, t_e, time instances for each rainfall event.
(c) The rainfall duration, d, can be obtained as the difference between the ending and beginning time instances as, $d = t_e - t_b$.
(d) The difference between rainfall amounts at the beginning and ending instances yields the total rainfall amount during the rainfall event, $(R_b - R_e)$.

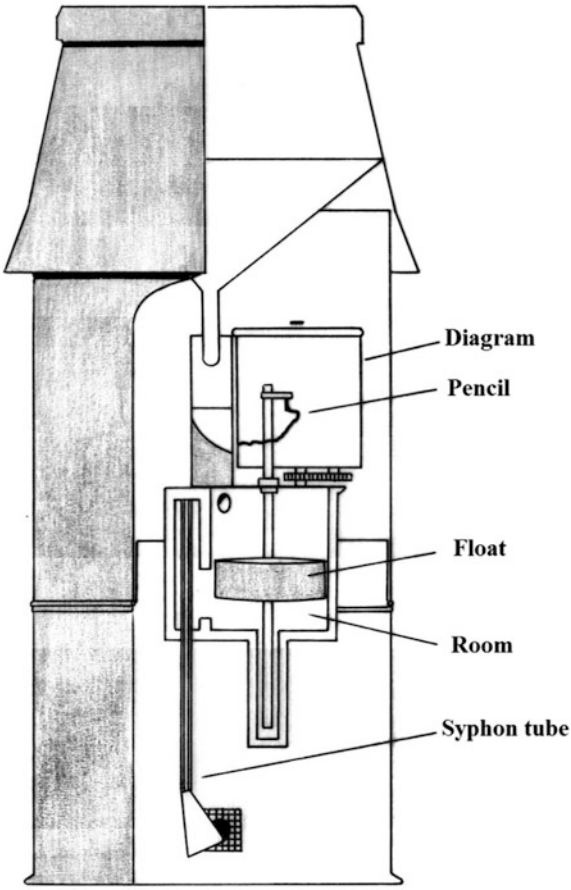

Fig. 2.10 Recording raingauge

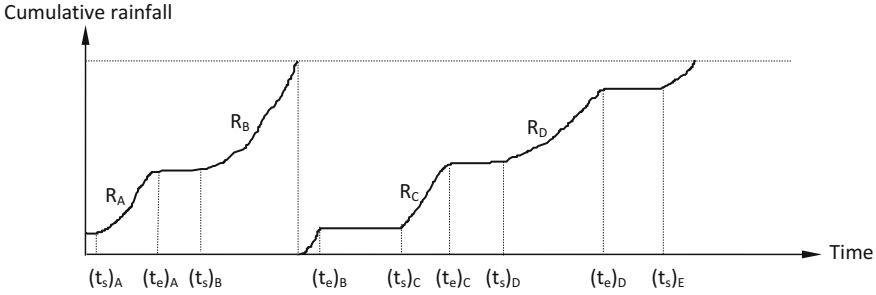

Fig. 2.11 Recording raingauge chart

(e) At each point on the rainfall chart trace, the slope of the tangent is equal to the rainfall intensity. It is possible to depict a certain time interval, Δd, much smaller than the rainfall duration, d, and starting from the rainfall occurrence during the whole rainfall duration, non-overlapping but adjacent Δd intervals will have corresponding rainfall increments, ΔR, and hence, the rainfall intensity can be calculated simply as $\Delta R/\Delta d$, which yields a set of intensities and the maximum value is adapted for design purposed in future activities. This point will be explained in detail in Sect. 2.12.

2.5 Rainfall Measurement Errors

In practice, it is not possible to measure rainfall amount without error. The best is to care with extra effort and record the measurement as errorless. However, the same care must be kept for each measurement, which is not possible in practice. Temporal or spatial arithmetic average rainfall amounts may have relatively less error than individual records. In practice, the location of the instruments must be selected in such a way that the overall recording errors are minimized as much as possible. There are three most significant error sources from the instruments.

(a) Errors from long-duration (daily or more) rainfall records: Possible evaporation from the raingauge is one of the major errors, which can be minimized by extra precautions to reduce its rate. For instance, addition of very fine layer of oil in the rainwater storage tank is one of the simple solutions.
(b) Errors from delay in transportation of rainfall water entrance: The rainfall water that falls on the funnel area may accumulate and cause entrance delay into the main water storage tank.
(c) Errors from icing: In cold weathers, water vapor in the air may freeze on the surface of the funnel and its hindrance of water entrance into the main water storage may cause errors.

Apart from these errors, there may be additional ones, because of the location change of the raingauge. In the establishment of the raingauge at a location, one must consider uniform rainfall around the instrument over 100 m or preferably 1000 m radius area without any hindrance to disturb such a uniform areal distribution (Fig. 2.12). A raingauge is rather a big body; therefore, it must be located in such a way that there must not be any increase or decrease error effect within the boundary layer.

Air masses may cause turbulence effects around the raingauge and, hence, may hinder vertical entrance of rainfall into the funnel part. Other hindrance structures such as buildings, walls, and trees do not allow rainfall to fall vertically into the funnel, and hence, reliable measurements cannot be recorded. In the fixation operations of raingauge location, these points must be taken into consideration.

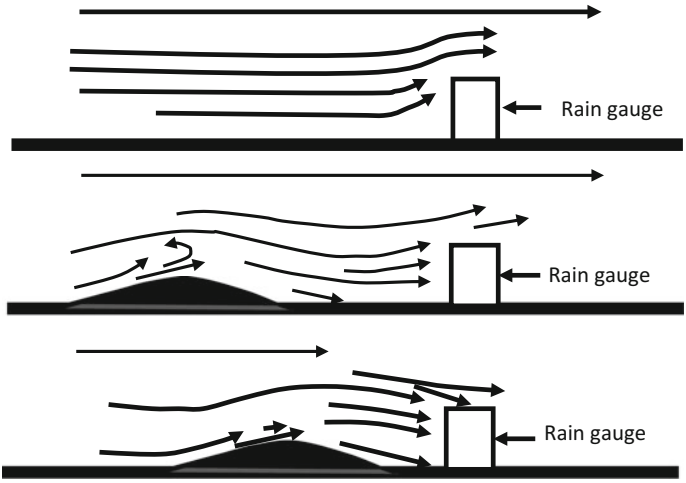

Fig. 2.12 Air flow around raingauges

In order to reduce the effect of the turbulence, the upper rim of the raingauge must be almost conveniently at the same level with the ground surface, but this may cause to other two error sources. The first one is that the splash of rain drops from the soil may enter the gauge, because of the indetermination of the convenient rim height from the earth surface. As stated earlier, high structures around the gauge may give rise to air movement disturbances and reliable measurements cannot be recorded. Such errors may be reduced if the rim of the raingauge is such that within the 30° space from the gauge, there are not structures as shown in Fig. 2.13.

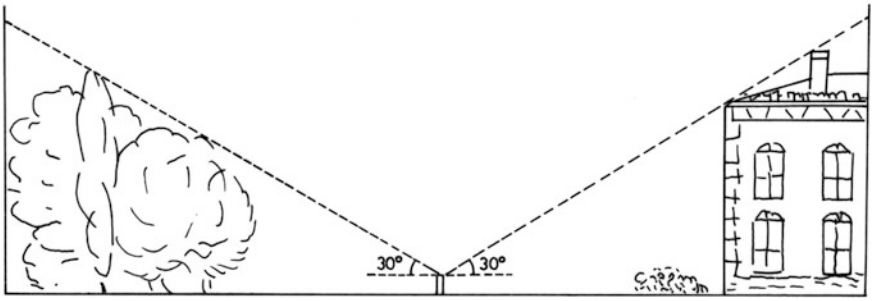

Fig. 2.13 Distance to adjacent hindrances

2.6 Arid Region Rainfall

Rainfall consists of the water drops that reach the Earth surface from clouds after cooling and condensation of atmospheric vapor. It is the sole source of surface and groundwater resources, and in particular, groundwater reservoirs are replenished after each shower of rainfall. For practical applications, the quantity of water that reaches the Earth surface from the clouds is important and it is expressed in height, depth, or weight as records of specified duration. In general, it is expressed, say, as length/time or weight/time, which is the rainfall intensity. The change of intensity during the rainfall occurrence provides significant information in many applications such as engineering water structure constructions and groundwater recharge. The major agent of the hydrology in any region is the rainfall, and in particular, in the arid and semiarid regions, its lack over extensive periods gives rise to aridity and water stress (Şen 2008). In particular, in the arid and semiarid regions, the most important rainfall features can be summarized as follows:

1. Rainfall can be very varied and erratic spatially and temporally.
2. Individual storm rainfall total can be very high, and in many cases, the single storm rainfall may exceed the mean annual rainfall leading to floods.
3. Rainfall intensities can be very high, and consequently, floods occur and groundwater recharge can be augmented significantly (Şen 2014).
4. The amount of runoff is increased by the scaling effects of rainfall impact, which increases runoff transport capacity and may lead to flood events.
5. Due to the seasonal pattern of the rainfall, erosion, sediment, and groundwater recharge yield follow similar pattern, where the most suitable period for these activities is the early part of the wet season, when the rainfall is high, but the vegetation has not grown sufficiently to protect the surface.
6. Weather patterns in arid regions are most often under the effect of small-scale orographic and convective rainfall occurrences rather than occasional large-scale frontal rainfalls.

Spatial rainfall variability is directly related to the local and regional topography. At high elevations, orographic rainfall occurs and this happens, especially, if surface water and nearby high hills exist within short distances from the sea coastal lines.

There are many days in arid zones without rainfall (zero rainfall) and groundwater recharge. The rainfall in arid zones usually pours down, and consequently, flash floods may pose risks even in the most desiccated desert regions. There are very scant flood records, and people in arid zones are aware of how to deal with these dangerous natural water hazards. Catastrophe may occur when a flash flood is unusually large, or when nothing has happened for such a long time that the settlers have been lulled into a false sense of security.

Surface runoff can be considered as one of the major problems in many regions. Surface flow-prone regions have many development projects, such as reclamation, agriculture, industry, tourism, settlements, and others. Runoff, especially in the

form of flash flood, is a real danger for the urban and social developments in these areas, and it is the main reason to lose big quantities of freshwater, besides the destruction of life stocks and water-related infrastructure.

The desert is characterized by rare rainfall occurrences, which normally do not increase more than 25 mm, annually. Rainfall in arid and semiarid zones results largely from convective cloud mechanisms producing storms typically of short duration, relatively high intensity, and limited areal extent (Cooke and Warran 1973). However, low-intensity frontal-type rains are also experienced, usually in the winter season. For instance, in the Red Sea area, relatively low-intensity rainfall may represent the greater part of annual rainfall during this period.

2.7 Rainfall Duration

Individual storm rainfall durations vary from climate belt to another, and for instance, the closer is the location to the equator, the longer is the rainfall event duration. In desert areas, it may vary between 1 hour and 6 hour, but in humid regions, the single rainfall event may continue even for many days.

In many regions of the world, especially in arid and semiarid regions, only daily precipitation measurements are available. Various types of depth–duration relationships have been developed to show rainfall distribution within storms. Such relationships vary a great deal depending on storm type. For example, orographic rainfalls will show a much more gradual accumulation of rainfall with time than will thunderstorm rainfalls. The maximum depth–duration relation of Fig. 2.14 is based on rainfall amounts in heavy storms averaged over areas ranging up to 1000 km^2 in Illinois, USA (Huff 1967). This relation arranges the rainfall increments for various time intervals in decreasing order of magnitude and not in chronological order. In other words, the curve, a depth–duration curve (24-hour probable maximum precipitation percentage relation to duration) shows the greatest 3-hour amount in the first 3 h, the second greatest 3-hour amount in the second 3-hour period, and so forth. This arrangement is not intended to represent the order in which the rainfall increments accidentally for an occasional storm. Studies of chronological distribution of rainfall within storms (the mass curve of rainfall) indicate no consistent pattern, with maximum intensities likely to occur during any period of the storm. The depth–duration curve in Fig. 2.14 is representative of convective storms in the central USA.

2.8 Missing Data Filling

In some of the meteorology stations, due to various reasons, sometimes the records cannot be kept properly and, therefore, cause to missing records. Among the main causes are the broken instruments, unreachable locations due to heavy meteorology

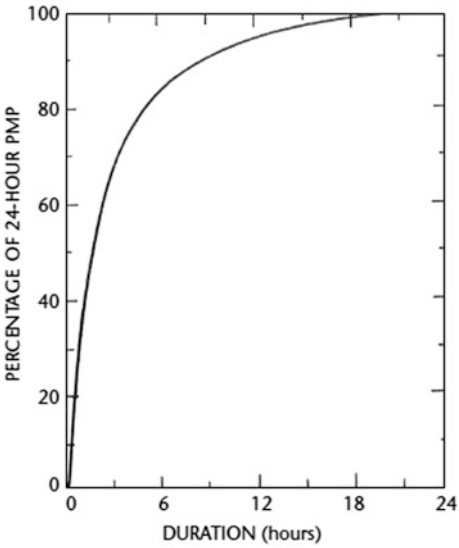

Fig. 2.14 Maximum depth-duration curve (Huff 1967)

conditions such as floods, intensive snow fall, terrorist activities, and alike. There are different methods for filling the missing records either within the record itself or among records at different locations. In the following sequel, missing record filling procedures are presented based on a set of stations.

2.8.1 Arithmetic Average

If the maximum relative error, α, among a set of adjacent stations is less than 10%, then areal arithmetic average can be thought as the representative missing rainfall filling procedure uniformly all over the study area. If the rainfall amounts at two stations are R_1 and R_2, then the relative error percentage is calculated by the following expression:

$$\alpha = 100\frac{|R_1 - R_2|}{\max(R_1, R_2)} \tag{2.1}$$

For the filling of missing station record, at least three adjacent station records must be taken into consideration. In the arithmetic average method, each station has the same weight, which is 1/n, where n is the number of stations in the arithmetic average calculation.

2.8.2 Ratio Method

If the relative errors among the stations are more than 10%, then arithmetic average method is not valid. One can select the way of weighting the rainfall amounts at adjacent stations. The missing record value is a function of the same time records at other stations with weighting factors that are the ratio of the missing station arithmetic average to the arithmetic averages of other stations. The missing station arithmetic average is $\overline{R}_X$, and other stations' arithmetic averages are $\overline{R}_A, \overline{R}_B$ and $\overline{R}_C$; additionally, if the rainfall amounts at adjacent stations are R_A, R_B, and R_c, the station weights are $\frac{\overline{R}_X}{\overline{R}_A}, \frac{R_X}{\overline{R}_B}$ and $\frac{R_X}{\overline{R}_C}$. Hence, the missing rainfall amount can be calculated as follows:

$$R_X = \frac{1}{3}\left(\frac{\overline{R}_X}{\overline{R}_A}R_A + \frac{\overline{R}_X}{\overline{R}_B}R_B + \frac{\overline{R}_X}{\overline{R}_C}R_C\right) \tag{2.2}$$

In case of more than three stations, this expression can be expanded similarly with the addition of new stations. In practical applications, calculations based on three stations are considered as sufficient for the application of the ratio method. In case of three stations, with almost equal arithmetic averages that are not different from each other more than 10% Eq. (2.2) reduces to the following arithmetic average expression with equal weights, 1/3:

$$R_X = \frac{1}{3}(R_A + R_B + R_C) \tag{2.3}$$

2.8.3 Inverse Distance Square Method

In the previous missing data filling procedures, the distances are not taken into account between the missing data station and the adjacent ones. In general, the closer the stations, the higher are their effects on each other. The missing data station location is taken as the origin point of a Cartesian coordinate system, and then, the closest station within each quadrant (I, II, III or IV) is considered for data filling procedure (Fig. 2.15).

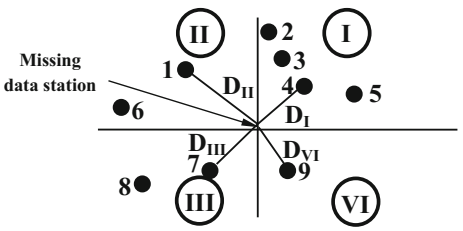

Fig. 2.15 Closest four stations

The closest four station distances to the origin point are D_{I}, D_{II}, D_{III}, and D_{VI} with the corresponding rainfall amounts R_{I}, R_{II}, R_{III}, and R_{IV}, and hence, the inverse distance square method missing data procedure equation is:

$$R_{\mathrm{X}} = \frac{\frac{1}{D_{\mathrm{I}}^2}R_1 + \frac{1}{D_{\mathrm{II}}^2}R_2 + \frac{1}{D_{\mathrm{III}}^2}Y_3 + \frac{1}{D_{\mathrm{IV}}^2}Y_4}{\frac{1}{D_{\mathrm{I}}^2} + \frac{1}{D_{\mathrm{II}}^2} + \frac{1}{D_{\mathrm{III}}^2} + \frac{1}{D_{\mathrm{IV}}^2}} \tag{2.4}$$

2.8.4 Correlation Method

A scatter diagram is obtained by plotting the two rainfall time series against each other with corresponding records. The most suitable straight line, if possible, is fitted to this scatter diagram. Such a straight-line indicates the correlation coefficient as the slope of the trend line. The fitting of the straight-line is achieved by least squares procedure. After the straight-line equation, one can obtain the missing rainfall value corresponding to available rainfall record at the same time in the next time series. In some cases, instead of a straight line, a nonlinear equation can be valid. If the records at two different locations are X_1, X_2, X_3, …, X_n and Y_1, Y_2, Y_3, …, Y_n, their scatter may take the form as in Fig. 2.16.

In the case of a straight line, one can obtain a and b parameters of the following mathematical function by statistical least squares technique (Benjamin and Cornell 1970):

$$Y = a + bX \tag{2.5}$$

According to the least squares technique, the straight line crosses through the arithmetic averages ($\overline{X}$ and $\overline{Y}$) of the two time series. This provides opportunity to take the arithmetic averages of the two sides in Eq. (2.5):

$$\overline{Y} = a + b\overline{X} \tag{2.6}$$

For determination of the two unknowns, it is necessary to have another equation The second expression can be obtained again under the light of the least squares

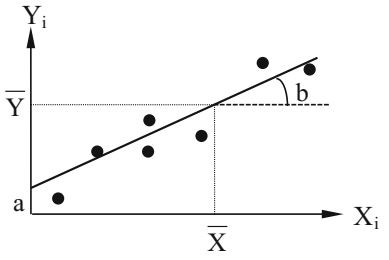

Fig. 2.16 Scatter diagram

method, after multiplying two sides of Eq. (2.5) by the independent variable, X, and then taking the arithmetic average of both sides leading to the following expression:

$$\overline{XY} = a\overline{X} + b\overline{X^2} \tag{2.7}$$

The cross multiplication of X and Y and its average, $\overline{XY}$, is the representative of the correlation coefficient that is also related to the regression coefficient. Furthermore, this correlation value is equivalent to the straight-line slope.

The coefficients a and b are calculated from the simultaneous solution of Eqs. (2.6) and (2.7) on the basis of two time series X_i and Y_i (i = 1, 2, 3, …, n). Equation (2.5) helps to fill the missing data in one of the time series, Y, from the other time series, X.

2.9 Double Mass Curve Method

In the rainfall records, there are two types of errors, namely systematic and random. The random errors are assumed to be embedded into the records with plus and minus signs. However, the random errors may not be very active in long-time series records. The major random errors are also referred to as the statistical sampling errors. Their sources can be explained along the following lines:

(a) Measurement errors from the instrument,
(b) Errors that originate from the writing and rounding,
(c) Printing errors, because rainfall records are distributed through the computer files or bulletins.

The systematic errors remain even on the long run, and therefore, they must be eliminated prior to any engineering calculations. The main systematic error sources are as follows:

(a) Station location shift: If the station location falls within the urban areal growth, dam reservoir coverage area, along the highway construction, then the station location must be shifted to another suitable location.
(b) Vegetation growth around the station and hindrance of wind: In such situations, the raingauge starts to measure more or less than the usual cases. The raingauge can be damaged due to animal hit and, hence, loses its sensitivity and starts to record systematic errors. Also, appearance of very small holes in the storage tank leads to systematic error records.
(c) Some pieces of the raingauge can be replaced by new ones, and hence, the new measurements may have slightly systematic error records.
(d) Various changes around the location of the raingauge may also lead to systematic errors.

In order to eliminate the systematic errors from the records, it is necessary to depend on the convenience tests. The most effective method for this purpose is the double mass curve graph analysis. The suspicious station values are shown on the vertical axis.

The application of the double mass curve method requires a set of adjacent station daily, monthly, or yearly record arithmetic averages together with the arithmetic averages of the suspicious station on the same durations. Generally, it is preferable to consider the station locations that fall within the same drainage basin or under the similar climatological region around the suspicious station. After the identification of the suspicious station, historically the last record average is considered as the first value in the sequence of averages with others following backward in a sequence. This implies that the last record comes at the end of the sequence. The averages of the suspicious station and the regional averages of the adjacent stations are plotted against each other on a Cartesian coordinate system as in Fig. 2.17.

If a single straight line is fitted to the scatter of points, then there is no systematic error in the suspicious meteorology station records. This implies that all the stations abide with homogeneity in the region. Otherwise, there appear broken straight lines, which is the indicator of systematic error in the suspicious station records. In this case, the slopes, α_1 and α_2, of the two straight lines are determined and the correction factor, f, for the records in the suspicious station can be calculated as,

$$f = \frac{\tan \alpha_1}{\tan \alpha_2} \tag{2.8}$$

Finally, all the records before the break point are corrected by multiplying each record by f. This leads to a single straight line on the scatter diagram with the corrected records.

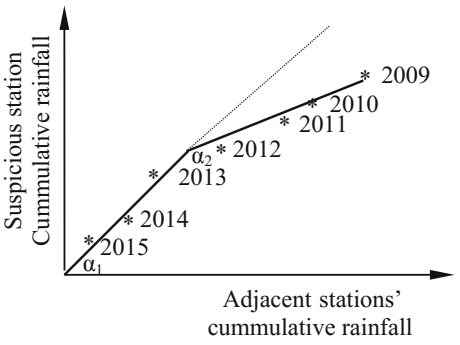

Fig. 2.17 Double mass curves

2.10 Rainfall Intensity

It is known from any textbook on principles of hydrology (Chow et al. 1988; Linsley 1986; Şen 2008) that a recording raingauge output graph gives the cumulative rainfall change during a storm by time (Fig. 2.12). For the sake of argument, the cumulative rainfall curve (CRC) is assumed in its simplest linear form with its slope, α, as in Fig. 2.18. At the storm beginning, it has the minimum

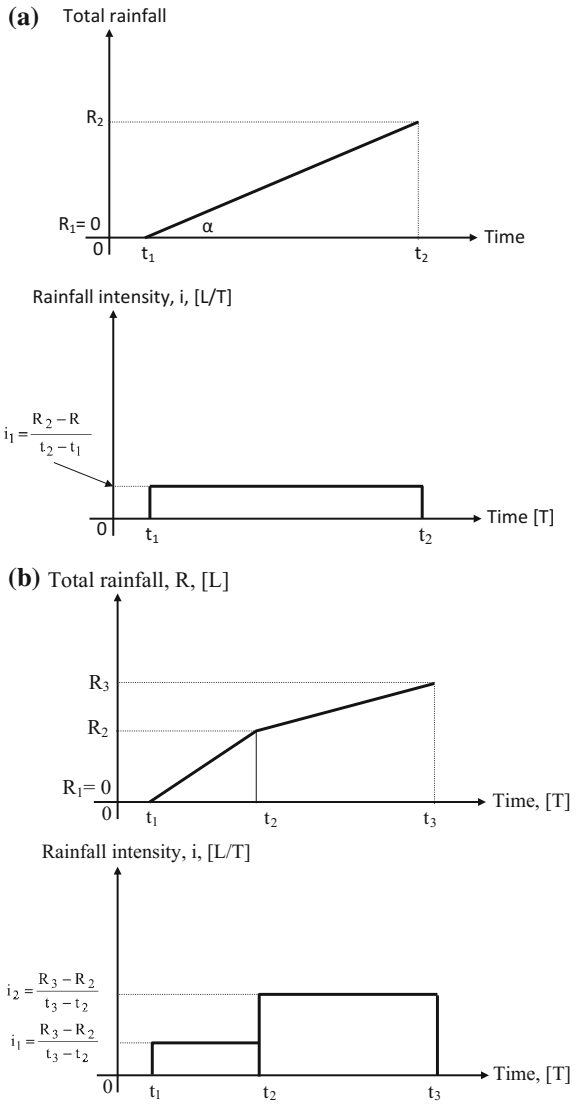

Fig. 2.18 Single storm rainfall record

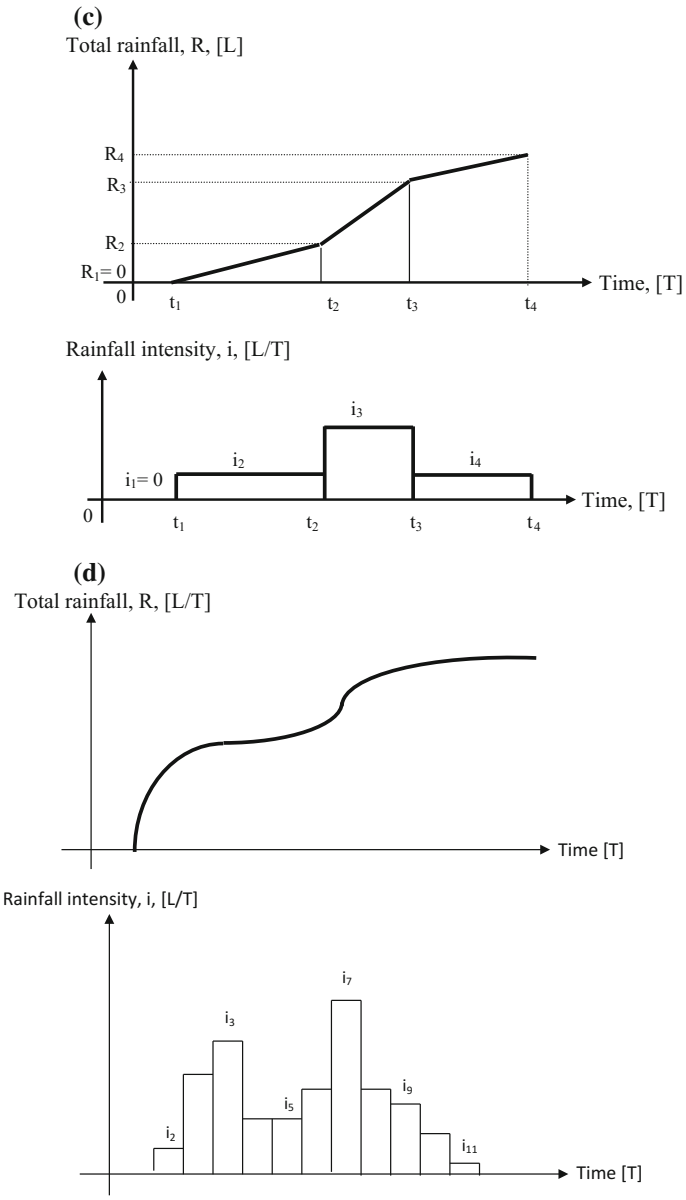

Fig. 2.18 (continued)

value ($R_1 = 0$), which reaches to its maximum at the end of the storm, R_2. If the storm rainfall has a uniform rate right from the beginning, t_1, until the end, t_2, of the storm, then it will appear as a straight line (see Fig. 2.18a).

The rainfall intensity, i, is equal to the slope of the total rainfall line, which is expressed geometrically as,

$$i = \tan \alpha \tag{2.9}$$

where α is the slope of CRC. It is also possible to express the rainfall intensity mathematically as the derivative of total rainfall amount, R, with respect to time, t, as,

$$i = \frac{\mathrm{d}R}{\mathrm{d}t} \tag{2.10}$$

which implies that the rainfall intensity is constant during dt duration. It is also possible to write the rainfall intensity in terms of a finite difference as,

$$i = \frac{R_2 - R_1}{t_2 - t_1} \tag{2.11}$$

In order to express simple change in the rainfall intensity, let us consider two straight lines that represent the CRC (see Fig. 2.18b). Accordingly, there are two rainfall intensities as, $i_1 = \mathrm{coc}\alpha_1$ and $i_2 = \mathrm{coc}\alpha_1$ or mathematically $i_1 = \mathrm{d}R_1/\mathrm{d}t$ and $i_2 = \mathrm{d}R_2/\mathrm{d}t$.

In general, there will be n small straight lines that can represent closely the CRC (see Fig. 2.18c), and hence, the corresponding rainfall intensities for each line are

$$i_1 = \mathrm{coc}\alpha_1, i_2 = \mathrm{coc}\alpha_1, i_3 = \mathrm{coc}\alpha_1, \ldots, \text{and } i_n = \mathrm{coc}\alpha_1 \tag{2.12}$$

or

$$i_1 = \mathrm{d}R_1/\mathrm{d}t, i_2 = \mathrm{d}R_3/\mathrm{d}t, i_3 = \mathrm{d}R_3/\mathrm{d}t, \ldots, \text{and } i_n = \mathrm{d}R_n/\mathrm{d}t \tag{2.13}$$

Similarly, a natural CRC will look like a non-decreasing curve, which will have relatively small slopes at the beginning and ending portions with comparatively bigger slopes in-between as in Fig. 2.18d. In order to convert the CRC into its hyetograph, it is necessary to divide the time axis into equal intervals, Δt, and then to find the corresponding rainfall increments from the vertical axis as ΔR_1, ΔR_2, …, ΔR_n. Accordingly, the rainfall intensities will be,

$$i_1 = \frac{\mathrm{d}R_1}{\Delta t}, i_2 = \frac{\mathrm{d}R_2}{\Delta t}, i_3 = \frac{\mathrm{d}R_3}{\Delta t}, \ldots, \text{and } i_n = \frac{\mathrm{d}R_n}{\Delta t} \tag{2.14}$$

If the rainfall intensity is plotted against the time increments, the resulting curve is the hyetograph, which shows the change of rainfall intensity by time (see Fig. 2.18d).

Example 2.1 The storm rainfall recording raingauge records on January 26, 2011, are given in Table 2.2. Since the length of minute-wise record is very long, the first two-hour records are presented in the table, but the whole record graph is shown in Fig. 2.19.

Table 2.2 Jeddah storm rainfall record

Date	mm	Time (min)	Cumulative rainfall (mm)	5-min	10-min	15-min	30-min	60-min	120-min
26/01/2011 10:57	0.1	1	0.1						
26/01/2011 10:58	0	2	0.1						
26/01/2011 10:59	0	3	0.1						
26/01/2011 11:00	0	4	0.1						
26/01/2011 11:01	0.1	5	0.2	1.2					
26/01/2011 11:02	0	6	0.2	1.2					
26/01/2011 11:03	0	7	0.2	1.2					
26/01/2011 11:04	0	8	0.2	1.2					
26/01/2011 11:05	0	9	0.2	0					
26/01/2011 11:06	0.1	10	0.3	1.2	1.2				
26/01/2011 11:07	0	11	0.3	1.2	1.2				
26/01/2011 11:08	0	12	0.3	1.2	1.2				
26/01/2011 11:09	0	13	0.3	1.2	1.2				
26/01/2011 11:10	0.1	14	0.4	1.2	1.2				
26/01/2011 11:11	0	15	0.4	1.2	1.2	1.2			
26/01/2011 11:12	0.1	16	0.5	2.4	1.8	1.6			
26/01/2011 11:13	0.1	17	0.6	3.6	2.4	2			
26/01/2011 11:14	0	18	0.6	2.4	2.4	2			
26/01/2011 11:15	0	19	0.6	2.4	1.8	1.6			
26/01/2011 11:16	0	20	0.6	1.2	1.8	1.6			
26/01/2011 11:17	0.1	21	0.7	1.2	2.4	2			

(continued)

Table 2.2 (continued)

Date	mm	Time (min)	Cumulative rainfall (mm)	5-min	10-min	15-min	30-min	60-min	120-min
26/01/2011 11:18	0	22	0.7	1.2	2.4	2			
26/01/2011 11:19	0.1	23	0.8	2.4	2.4	2.4			
26/01/2011 11:20	0	24	0.8	2.4	2.4	2			
26/01/2011 11:21	0	25	0.8	1.2	1.8	2			
26/01/2011 11:22	0.1	26	0.9	2.4	1.8	2.4			
26/01/2011 11:23	0	27	0.9	1.2	1.8	2.4			
26/01/2011 11:24	0	28	0.9	1.2	1.8	2			
26/01/2011 11:25	0.1	29	1	2.4	2.4	2.4			
26/01/2011 11:26	0	30	1	1.2	1.8	2	1.8		
26/01/2011 11:27	0.1	31	1.1	2.4	2.4	2	2		
26/01/2011 11:28	0.1	32	1.2	3.6	2.4	2.4	2.2		
26/01/2011 11:29	0.1	33	1.3	3.6	3	2.8	2.4		
26/01/2011 11:30	0	34	1.3	3.6	3	2.8	2.2		
26/01/2011 11:31	0	35	1.3	2.4	2.4	2.4	2.2		
26/01/2011 11:32	0.2	36	1.5	3.6	3.6	3.2	2.6		
26/01/2011 11:33	0.3	37	1.8	6	5.4	4	3.2		
26/01/2011 11:34	0.3	38	2.1	9.6	6.6	5.2	3.8		
26/01/2011 11:35	0.2	39	2.3	12	7.8	6	4		
26/01/2011 11:36	0.3	40	2.6	13.2	9	6.8	4.6		
26/01/2011 11:37	0.6	41	3.2	16.8	12	9.2	5.8		
26/01/2011 11:38	0.7	42	3.9	21.6	15.6	12	7.2		

(continued)

Table 2.2 (continued)

Date	mm	Time (min)	Cumulative rainfall (mm)	5-min	10-min	15-min	30-min	60-min	120-min
26/01/2011 11:39	0.8	43	4.7	28.8	20.4	14.8	8.6		
26/01/2011 11:40	0.6	44	5.3	32.4	24	17.2	9.8		
26/01/2011 11:41	0.7	45	6	33.6	27	19.6	11		
26/01/2011 11:42	0.5	46	6.5	31.2	28.2	21.2	11.8		
26/01/2011 11:43	1.1	47	7.6	34.8	33	25.2	14		
26/01/2011 11:44	1.7	48	9.3	48	42	32	17.4		
26/01/2011 11:45	1.5	49	10.8	57.6	49.2	38	20.4		
26/01/2011 11:46	1.6	50	12.4	70.8	55.2	43.6	23.4		
26/01/2011 11:47	1.3	51	13.7	73.2	58.8	47.6	26		
26/01/2011 11:48	0.8	52	14.5	62.4	58.8	49.6	27.4		
26/01/2011 11:49	0.5	53	15	50.4	58.2	50.8	28.4		
26/01/2011 11:50	0.2	54	15.2	33.6	55.2	50.4	28.8		
26/01/2011 11:51	0.3	55	15.5	21.6	54	49.2	29.2		
26/01/2011 11:52	1.2	56	16.7	26.4	54.6	51.2	31.6		
26/01/2011 11:53	1.9	57	18.6	43.2	55.8	55.6	35.4		
26/01/2011 11:54	1.5	58	20.1	58.8	55.8	59.2	38.2		
26/01/2011 11:55	1.2	59	21.3	69.6	53.4	61.2	40.6		
26/01/2011 11:56	1.6	60	22.9	74.4	55.2	65.6	43.6	22.8	
26/01/2011 11:57	1.3	61	24.2	67.2	58.2	66.4	46	24.1	
26/01/2011 11:58	1.5	62	25.7	67.2	64.2	65.6	48.8	25.6	
26/01/2011 11:59	1.6	63	27.3	72	72.6	66	52	27.2	

(continued)

Table 2.2 (continued)

Date	mm	Time (min)	Cumulative rainfall (mm)	5-min	10-min	15-min	30-min	60-min	120-min
26/01/2011 12:00	1.4	64	28.7	69.6	79.2	65.2	54.8	28.5	
26/01/2011 12:01	1.3	65	30	69.6	79.8	65.2	57	29.8	
26/01/2011 12:02	1.5	66	31.5	69.6	77.4	68	59.4	31.3	
26/01/2011 12:03	1.1	67	32.6	63.6	75	70.4	61	32.4	
26/01/2011 12:04	1.4	68	34	63.6	76.2	75.2	63.4	33.8	
26/01/2011 12:05	1.4	69	35.4	64.8	75	79.6	65.6	35.1	
26/01/2011 12:06	1.4	70	36.8	63.6	75.6	80.4	67.2	36.5	
26/01/2011 12:07	1.5	71	38.3	68.4	75.6	78.8	68.8	38	
26/01/2011 12:08	1.6	72	39.9	70.8	75.6	79.2	70.4	39.6	
26/01/2011 12:09	1.5	73	41.4	72	76.2	80.4	72.2	41	
26/01/2011 12:10	1.3	74	42.7	70.8	76.2	79.2	73.4	42.3	
26/01/2011 12:11	0.8	75	43.5	62.4	72	77.2	74	43	
26/01/2011 12:12	1.1	76	44.6	56.4	72	75.6	74	44	
26/01/2011 12:13	1	77	45.6	50.4	69.6	73.2	72.6	45	
26/01/2011 12:14	1.1	78	46.7	48	67.8	72	71.8	46.1	
26/01/2011 12:15	1.5	79	48.2	56.4	68.4	72.8	71.6	47.6	
26/01/2011 12:16	1	80	49.2	55.2	65.4	70.8	71	48.5	
26/01/2011 12:17	0.9	81	50.1	54	61.2	70	71.2	49.4	
26/01/2011 12:18	1.1	82	51.2	54	58.8	68.8	72.4	50.4	
26/01/2011 12:19	0.5	83	51.7	42	54	65.2	73	50.9	
26/01/2011 12:20	0.5	84	52.2	36	52.2	61.6	73.4	51.4	

(continued)

Table 2.2 (continued)

Date	mm	Time (min)	Cumulative rainfall (mm)	5-min	10-min	15-min	30-min	60-min	120-min
26/01/2011 12:21	0.9	85	53.1	36	51	59.2	72.8	52.2	
26/01/2011 12:22	0.6	86	53.7	30	48.6	55.2	70.2	52.8	
26/01/2011 12:23	0.2	87	53.9	26.4	43.2	50	67.6	53	
26/01/2011 12:24	0	88	53.9	20.4	34.2	44.8	65.2	52.9	
26/01/2011 12:25	0.1	89	54	10.8	28.8	42	62.2	53	
26/01/2011 12:26	0.2	90	54.2	6	24.6	38.4	60	53.1	
26/01/2011 12:27	0.2	91	54.4	6	19.2	35.2	57.4	53.2	
26/01/2011 12:28	0	92	54.4	6	16.2	30.8	54.2	53.1	
26/01/2011 12:29	0	93	54.4	4.8	13.2	24.8	51.4	53.1	
26/01/2011 12:30	0.1	94	54.5	3.6	8.4	21.2	49	53.2	
26/01/2011 12:31	0.1	95	54.6	2.4	5.4	18	46.2	53.1	
26/01/2011 12:32	0.3	96	54.9	6	6	14.8	44.6	53.1	
26/01/2011 12:33	0.4	97	55.3	10.8	8.4	14.4	42.6	53.2	
26/01/2011 12:34	0.2	98	55.5	12	9	13.2	40.2	53.2	
26/01/2011 12:35	0.4	99	55.9	15.6	10.2	11.2	38.2	53.3	
26/01/2011 12:36	0.7	100	56.6	20.4	13.2	11.6	36.6	53.4	
26/01/2011 12:37	0.8	101	57.4	25.2	18	14	35	53.5	
26/01/2011 12:38	0.7	102	58.1	31.2	22.2	16.8	33.4	53.4	
26/01/2011 12:39	1.3	103	59.4	42	29.4	21.6	33.4	54.1	
26/01/2011 12:40	1.4	104	60.8	50.4	37.2	26.4	34.6	54.8	
26/01/2011 12:41	1.5	105	62.3	58.8	44.4	31.6	35.4	55.8	

(continued)

Table 2.2 (continued)

Date	mm	Time (min)	Cumulative rainfall (mm)	5-min	10-min	15-min	30-min	60-min	120-min
26/01/2011 12:42	1.6	106	63.9	69.6	51.6	38	36.6	56.3	
26/01/2011 12:43	1.5	107	65.4	72	59.4	44	37.4	56.1	
26/01/2011 12:44	0.8	108	66.2	64.8	61.8	46.8	36	55.4	
26/01/2011 12:45	0.8	109	67	56.4	62.4	49.6	35.6	54.6	
26/01/2011 12:46	1	110	68	49.2	63.6	52.4	35.8	54.3	
26/01/2011 12:47	1.6	111	69.6	50.4	69	57.2	36.8	55.1	
26/01/2011 12:48	1.3	112	70.9	56.4	69	61.6	38.4	55.9	
26/01/2011 12:49	1.3	113	72.2	62.4	68.4	65.2	40	57	
26/01/2011 12:50	0.5	114	72.7	56.4	62.4	64.4	39.2	57.2	
26/01/2011 12:51	0.9	115	73.6	48	58.2	64.8	39.8	56.9	
26/01/2011 12:52	0.8	116	74.4	42	54	65.2	41	55.8	
26/01/2011 12:53	0.6	117	75	33.6	52.8	62.4	42.2	54.9	
26/01/2011 12:54	0.4	118	75.4	32.4	50.4	58.4	42.8	54.1	
26/01/2011 12:55	0.3	119	75.7	25.2	46.2	53.6	43	52.8	
26/01/2011 12:56	0.2	120	75.9	18	37.8	48	43	51.7	37.9

The relationship between the rainfall intensity and the duration is given in Fig. 2.19, where the rainfall intensity (the slope of the tangent at any point) starts as high values and by the time decreases.

The variation of rainfall amount during the storm rainfall is shown in Fig. 2.20. It is obvious that especially between the first 50–70 min, the rainfall height is the maximum.

The rainfall intensity calculations are presented in Table 2.2 for 5-, 10-, 20-, 30-, 60-, and 120-min durations; the maximum rainfall intensity during each one of these durations is plotted against the selected durations; and the result is given in Fig. 2.21, where a straight line is matched through the scatter points on the double logarithmic paper.

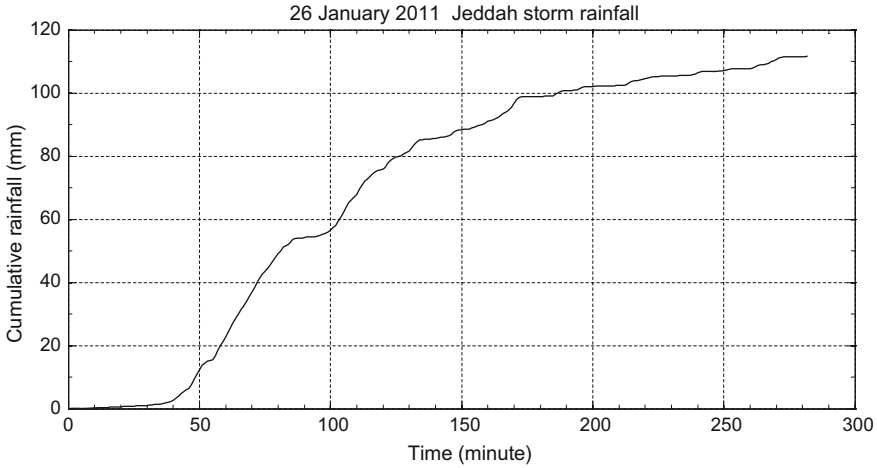

Fig. 2.19 Cumulative rainfall amounts during 26 January 2011 Jeddah storm rainfall

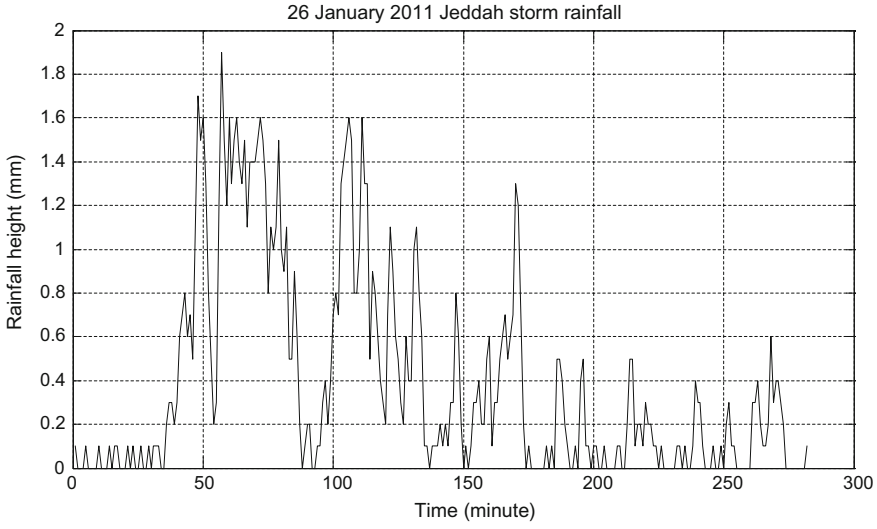

Fig. 2.20 Jeddah storm rainfall time series

2.11 Hyetograph–Hydrograph Relationship

The rainfall intensity at the earth's surface splits into two parts, namely losses of infiltration, evaporation, depletion, and runoff. They are referred to as non-effective (losses) rainfalls and effective (runoff). As shown in Fig. 2.22a, the upper (effective) part corresponds to direct runoff and the lower (non-effective) part leads to infiltration and later to the consequent groundwater recharge. In Fig. 2.22a, the division

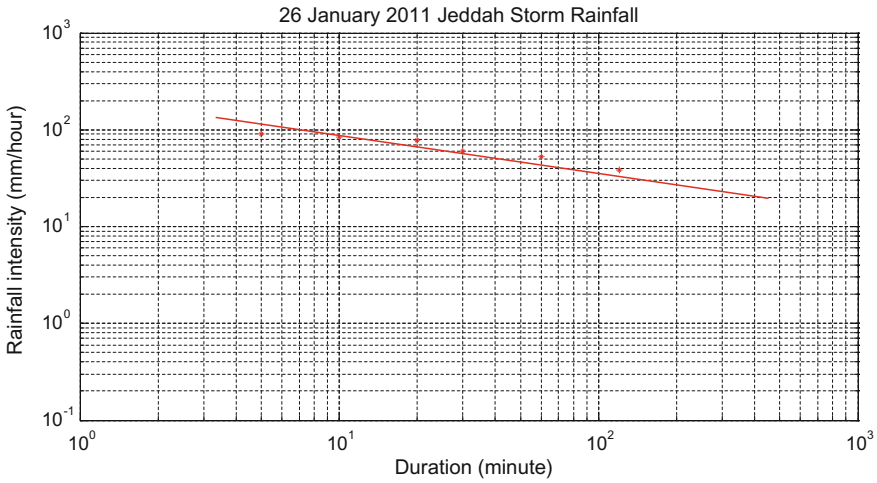

Fig. 2.21 Rainfall intensity–duration curve

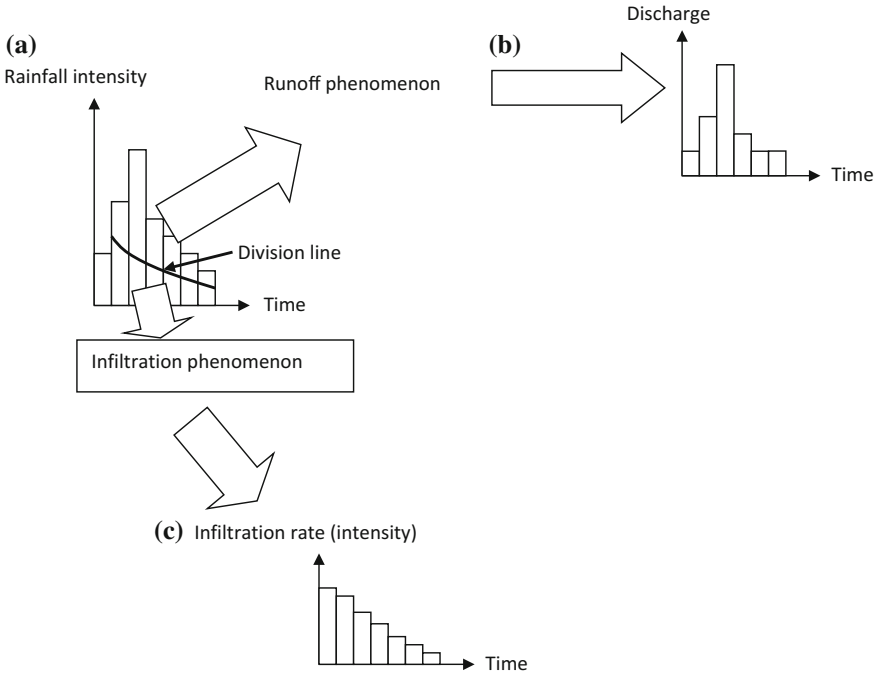

Fig. 2.22 (**a**) Hyetograph, (**b**) hydrograph, and (**c**) infiltration curve

line is located rather arbitrarily, but in actual studies, it corresponds to the infiltration curve (Şen 2008). Hydrograph is the graphical form of effective rainfall change on the earth's surface, whereas infiltration curve is the graphical appearance of non-effective rainfall time variation in the subsurface.

In hyetograph and infiltration curves, the vertical axis is shown as the rainfall intensity, whereas the hydrograph has the vertical axis allocated for discharge dimension. The drainage area, A, plays the main role as the conversion factor between the discharge and the rainfall intensity or infiltration rate. The hyetograph is the summation of hydrograph and infiltration curve.

Similar to rainfall event, infiltration also changes with time and infiltrometers are used to record the cumulative water that enters the earth surface by time. The reader is referred to any basic textbook on the hydrology principles for detailed information on infiltrometers (Chow et al. 1988; Şen 2008). Herein, the procedure of calculations and the derivation of the infiltration graph are explained explicitly. Similar to CRC, total infiltration curve is obtained in the field by infiltration test measurements. In the case of assumed uniform infiltration rate from the beginning (t_b) of the test until the soil is saturated, i.e., ending time (t_e) of infiltration, a similar straight line appears as in Fig. 2.18a (see Fig. 2.23a).

By definition, the infiltration rate, f, is the slope of this straight line and trigonometrically it is possible to write,

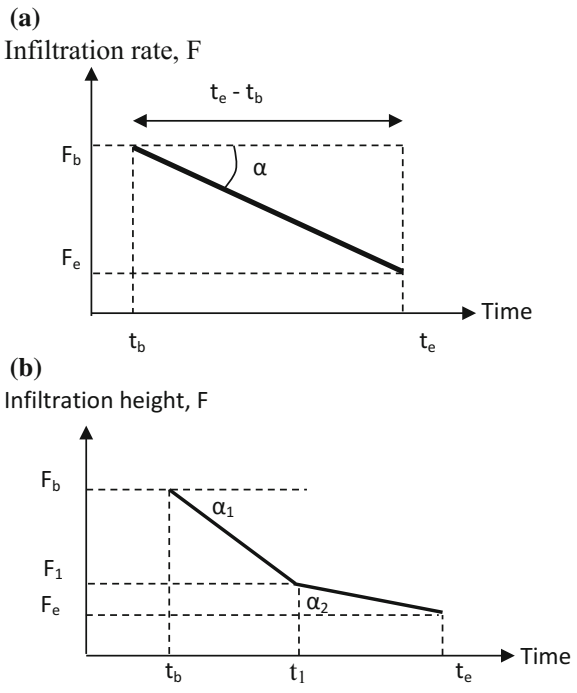

Fig. 2.23 Uniform infiltration rate

$$f = \tan\alpha \tag{2.15}$$

or

$$f = \frac{F_e - F_b}{t_e - t_b} = \frac{df}{dt} \tag{2.16}$$

In the case of heterogeneous infiltration rate, there are at least two straight lines that represent the infiltration rate curve as shown in Fig. 2.23b, but the second straight line is expected physically to have smaller slope than the first one. This is due to the fact that as the time passes the soil becomes more saturated and accommodates less water by time. Any infiltration curve starts with a big slope, which becomes smaller by time, and finally, it remains the same indicating that the soil cannot accommodate additional water, since it is completely saturated. The infiltration rates can be calculated as $f_1 = \tan\alpha_1$ and $f_2 = \tan\alpha_2$ or $f_1 = dF_1/dt$ and $f_2 = dF_2/dt$. However, if there are n different straight lines, the infiltration rates can be calculated as $f_1 = \tan\alpha_1$, $f_2 = \tan\alpha_2$, $f_3 = \tan\alpha_3$, …, and $f_n = \tan\alpha_n$ or according to Eq. (2.16) $f_1 = dF_1/dt$, $f_2 = dF_2/dt$, $f_3 = dF_3/dt$, …, $f_n = dF_n/dt$. After the infiltration test in the field and the completion of necessary calculations, it is possible to obtain an exponential curve according to Horton (1933) as in Fig. 2.24.

By considering the same time intervals, one can calculate the rainfall intensity values that cause to direct runoff, by the subtraction of the infiltration from the same time interval rainfall intensity, r, which leads to,

$$i_1' = i_1 - f_1, i_2' = i_2 - f_2, i_3' = i_3 - f_3, \ldots, i_n' = i_n - f_n \tag{2.17}$$

Finally, the residual hyetograph that leads to direct surface runoff becomes as in Fig. 2.25.

In practical works, the histogram is divided into two parts by a horizontal line such that the overlying hyetograph area is equal to direct runoff height. This is referred to as the Φ-index method (Chow et al. 1988; Linsley et al. 1988). In the last graph of Fig. 2.25, the remaining effective rainfall, which is the cause of direct runoff, is converted into a rectangle with the same area of the hyetograph by leaving the base time the same. This yields the height of the equivalent rectangle with an

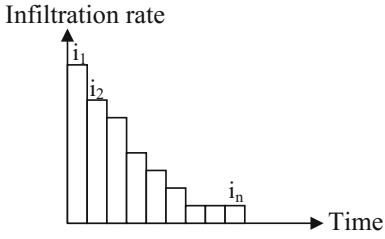

Fig. 2.24 Infiltration rate curve

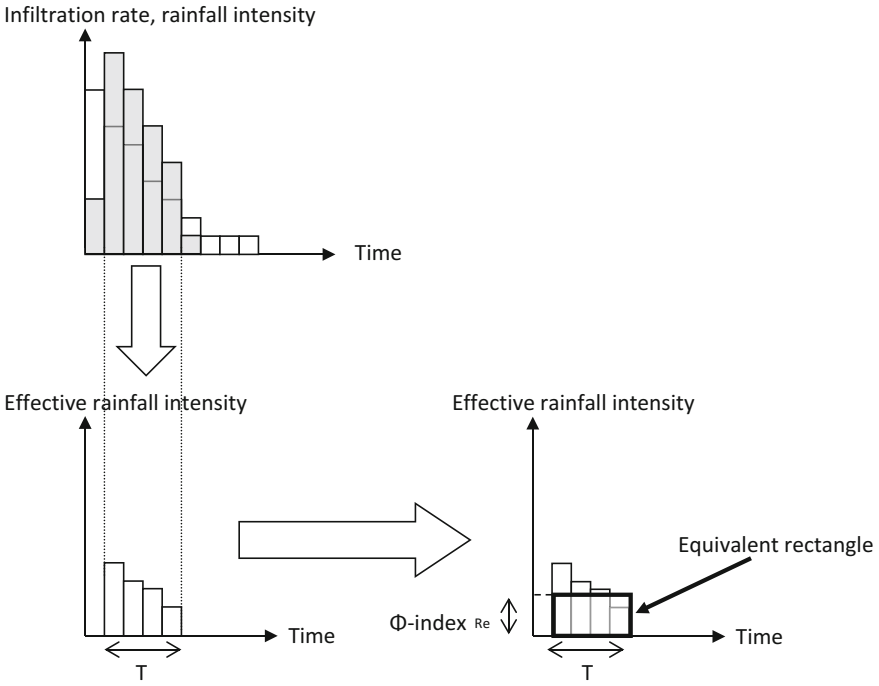

Fig. 2.25 Direct hyetograph

effective rainfall height, R_e or Φ-index, that should be considered in any hydrograph analysis.

It is now time to consider the transformation mechanics of the direct hyetograph into its direct hydrograph through the watershed properties. This information will be used in Chap. 4 following sections for arriving at a proper hydrograph according to some assumptions or empirical relationships. The transformation has two phases: The first one is concerned with time translation, because in nature, the hydrograph peak discharge always appears after the end of effective rainfall (shifting principle in Chap. 4). The second phase is due to the storage effect of the watershed area, which gives different shapes to the hydrograph at different sections, and hence, the peak of the hydrograph also changes In general, the highest effective rainfall in the hyetograph is higher than the depth of the peak direct hydrograph discharge.

By definition in any direct hydrograph, the area under the curve, which corresponds to direct rainfall volume, is equal to the multiplication of the watershed area, A, by idealized average effective rainfall height, R_e. Depending on what have been explained above, one can deduce the following significant quantities for further hydrograph analysis:

1. Effective rainfall amount, R_e,
2. Effective rainfall duration, t_e,
3. Hydrograph peak discharge, Q_p,
4. Time to peak discharge, t_p,
5. Hydrograph base time duration, t_b,
6. The time lag, t_L, in the sense of distance between the effective rainfall centroid and the hydrograph peak.

First two quantities are completely related to rainfall and infiltration properties. Infiltration is dependent on the type of soil, vegetation, land use, and geology. The third, fourth, and fifth quantities are functions of rainfall and watershed characteristics. The last point is related to the response of watershed to rainfall as input. The time lag can be expressed by different conceptions. For instance, it may be taken as the time difference between the centroids of hyetograph and hydrograph. However, commonly it is taken as the time difference between the centroid of hyetograph and peak hydrograph discharge. These are the key information in any hydrograph calculation. In theoretical or synthetic hydrograph analysis, each one of these factors is simplified or expressed in terms of measurable watershed characteristics.

2.12 Intensity–Duration–Frequency (IDF) Curves

In the planning and assessment of any water resources, IDF curves have fundamental importance. In the literature, there are numerous theoretical and empirical approaches for their constructions (Chow et al. 1988; Bell 1969; Aron et al. 1987; Burlando and Rosso 1996; Koutsoyiannis et al. 1998). The regional studies of IDF curves are given for some countries (Froehlich 1995a, b, c; Garcia-Bartual and Schneider 2001).

In many humid areas of the world, IDF curves are constructed on the basis of Gumbel theoretical PDF (Gumbel 1958; Chap. 6). However, in arid and semiarid lands, Gamma PDF is more convenient. In the construction of IDF curves, the following meaningful knowledge, information, and interpretation are important:

1. Any PDF indicates the symmetric or skew distribution features of the rainfall records. For instance, in dry regions as climate knowledge, low (high) rainfall occurrences appear at high (low) frequency. Such situations are representative by the Gamma PDF or its version as exponential PDF (Chap. 6).
2. In water engineering, IDF curves are calculated frequently for 2-, 5-, 10-, 25-, 50-, and 500-year design durations in risk assessments.

If the rainfall intensity is denoted by i and the IDF curve function is denoted by $f(i)$, then it is shown in an integral form, the risk, r, is defined as,

$$r = \int_{i}^{+\infty} f(i)\mathrm{d}i \tag{2.18}$$

In the derivation of IDF curves, another point is the relationship between storm rainfall duration, T, and the maximum rainfall intensity, i.

Many procedures and formula, mainly empirical, are proposed in the literature for IDF curve identification (Yarnell 1935; Chow et al. 1988; Gumbel 1958; Bell 1969; Chen 1983; Aron et al. 1987). A mathematical approach is proposed by Burlando and Rosso (1996) and Koutsoyiannis et al. (1998). In practice, division of the rainfall duration into three groups, namely durations from 1 min to 1 h as "short," from 1 to 24 h as "intermediate," and more than 24 h as "long," has led to meaningful interpretations and works on the regionalization of IDF relationships in different geographical areas (Froehlich 1995a, b, c; Hanson 1995; Garcia-Bartual and Schneider 2001). In many parts of the world, the recording raingauge instruments are either rarely available or not at all. For these regions, the IDF curves can be obtained through empirical approaches (Chow et al. 1988). Proper and accurate determination of IDF curves is possible if the storm rainfall accumulation records are available.

In the literature, the most used three formulations with two-parameter mathematical functions are summarized as follows:

1. The most widely used expression with R and C (two-parameter) is due to Sherman (1931) as,

$$i = \frac{R}{T + C} \tag{2.19}$$

2. Bernard (1932) provided a hyperbolic expression again with two parameters as,

$$i = \frac{R}{T^{\mathrm{C}}} \tag{2.20}$$

3. The relationship between the intensity and duration on a semilogarithmic paper appears as a straight line.

$$i = R - CLnT \tag{2.21}$$

On the other hand, there are also three-parameter functions. Similar to Eqs. (2.20) and (2.25) with a third parameter, B,

$$i = \frac{R}{(T+C)^{\mathrm{B}}} \tag{2.22}$$

and

$$i = \frac{R}{T^{\mathrm{B}} + C} \tag{2.23}$$

Other three-parameter equations are given by Garcia-Bartual and Schneider (2001) as,

$$i = R + \frac{B}{T+C} \tag{2.24}$$

and

$$i = \frac{R}{B+CT} \tag{2.25}$$

Keers and Wescott (1977) suggested the following formulation:

$$i = \frac{R}{(1+BT)^{\mathrm{C}}} \tag{2.26}$$

The IDF relationships are of fundamental importance in hydrology for flood assessments, especially in engineering water structure designs. These curves are necessary for design storm determination and also as prerequisites in many hydrological models and procedures for design discharge computation. Flood risk evaluation and mitigation works also necessitate IDF information in order to plan appropriate infrastructures including rainfall drainage systems, dam spillways, culverts, bridges, levees, dikes for protecting local settlers and their properties against flood danger with efficiency.

In this section, determination of convenient IDF curves is presented based on the annual daily maximum rainfall (DMR) records. For this purpose, a dimensionless intensity–duration (DID) curve is derived from the available recording raingauge and then the theoretical probability distribution function (PDF) is fitted to DMR data. The PDF provides opportunity to determine the DMR amounts corresponding to a set of return periods (2, 5, 10, 25, 50 and 100 year). The DID curve helps to disaggregate the DMR amounts to a set of shorter rainfall duration (10, 20, 30, 60, 120, 360, 720 and 1440 min).

In many parts of the world, past and current IDF statistics are computed by considering the Gamma, log-normal, extreme value (Gumbel), generalized extreme value (Pearson), and Weibull PDF to describe the frequency of extreme rains. These theoretical PDFs are also used by most of the official meteorological services in different countries. The Gumbel and Pearson PDFs have the advantage to be well

known by the engineering communities for the works on the reliability of hydraulic infrastructures.

The rainfall regime in arid and semiarid regions does not abide by the Gumbel cumulative distribution function CDF. In almost all applications, Gumbel CDF is employed theoretically due to either nonexistence of basic data or convenience of use or both. This is the main reason why after flood events there are damages to hydraulic structures such as bridges, culvers, and levees, especially in arid lands. It is, therefore, necessary to assess the IDF properties of storm events leading to convenient curves even though the basic data may not be very sufficient.

In this section, the determination of convenient IDF curves is presented for the Kingdom of Saudi Arabia (KSA) as a representative of arid regions. Various CDFs have been used on the basis of factual data for a set of time durations such as 5, 10, 15, 20, 30, and 60 min. On the basis of these CDFs, the possible rainfall intensities for a set of design periods (return periods or risk levels) are presented by considering 2-year, 5-year 10-year, and 25-year, 50-year, 100-year, and 500-year durations (SGS, 1015).

2.12.1 Dimensionless Intensity–Duration (DID) Curve

In the previous section, most frequently used theoretical intensity duration (ID) formulations are presented, and depending on the parameter values, each one yields a single curve. If the parameters are determined in some way, then this single curve can be converted into a DID curve after dividing the duration (intensity) values by the maximum duration (intensity) value. With hypothetical values of $A = 200$, $B = 0.8$, and $C = 4$ the resulting DID curves appear for different formulations as in Fig. 2.26.

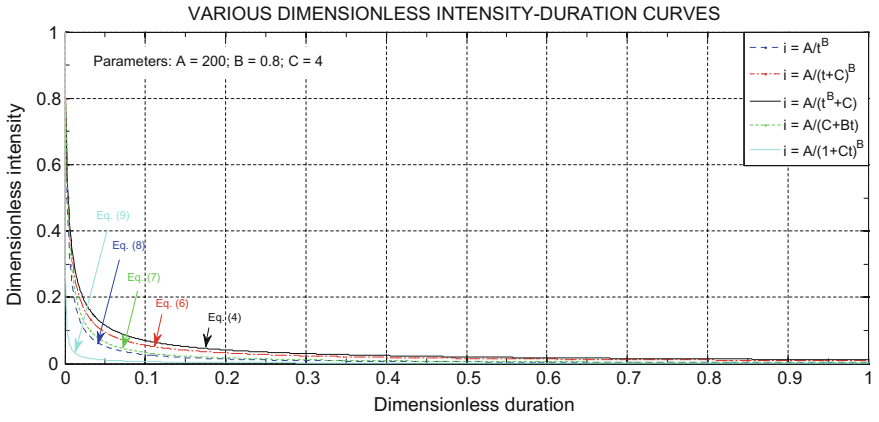

Fig. 2.26 Dimensionless intensity–duration curves

Different sets of parameter values yield slight shifts in these curves, but their general shape remains the same.

The view adopted in this section is that all ID curves for different return periods fall on the same DID curve. Hence, once DID curve is obtained, then it is possible to obtain all of the actual intensity–duration curves for any given return period or exceedence probability (frequency) provided that the DMR data are available.

2.12.2 *Intensity–Duration–Frequency (IDF) Curve Generation*

It is necessary to consider that an IDF curve provides numerical information about the intensity and the return period (inverse of exceedence probability) (Chap. 6). On the basis of this sentence, the questions are "how can one obtain a set of intensities for a given set of return periods at certain duration?" and "what might be this duration?" In practice, most often the total daily rainfall amounts are available and they can be converted to DMR records, which imply rainfall duration as one day, i.e., 1440 min. In arid and semiarid regions, one cannot observe day-long rainfall events, because they have shorter duration. In such regions, depending on the location, one can take the DMR durations as 3 or 6 hours. Whatever the duration, one can obtain the theoretical PDF of the DMR data and then a set of exceedence probability rainfall amounts can be calculated each attached with the return periods. After the calculation of these rainfall amounts for a given duration, the remaining is to disaggregate them into shorter time durations by means of DID curve.

For IDF curves, generation from the DMR amounts and their combination with the DID curve can be achieved through the execution of the following steps:

1. Since DMR amounts for 6 hours = 360 min are available, first the most suitable PDF is determined for each station,
2. The theoretical PDFs help to calculate rainfall amounts that correspond to a set of desired probabilities of exceedence, p, according to the inverse relationship between the return period, T, and the probability of exceedence, p, as $p = 1/T$. The return period (exceedence probability) set is adapted as T = 2-year (p = 0.50), T = 5-year (p = 0.20), T = 10-year (p = 0.10), T = 25-year (p = 0.04), T = 50-year (p = 0.02), and T = 100-year (p = 0.01),
3. The IDF curves can be generated on the basis of the available information from the previous steps concerning DMR data and DID curve. Additionally, one should also know rainfall amount corresponding to the exceedence probability for each return period from the suitable PDF for each station,
4. Available natural IDF curves from different parts of the KSA are converted to DID curves as in Fig. 2.27 with the best average DID curve expression as,

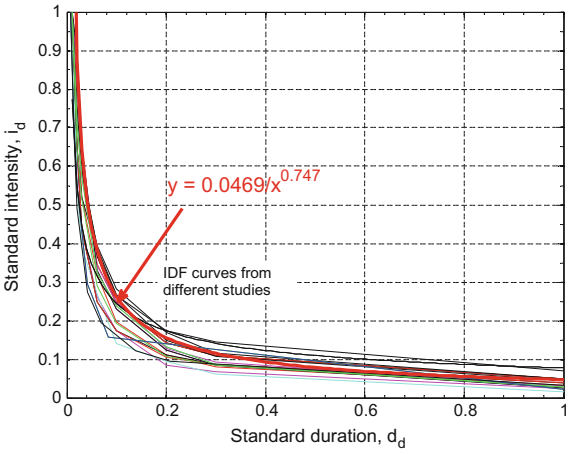

Fig. 2.27 Dimensionless intensity–duration curves

$$i_{\mathrm{d}} = \frac{0.0469}{d_{\mathrm{d}}^{0.747}} \tag{2.27}$$

where i_{d} and d_{d} are dimensionless intensity and duration, respectively.

5. Since definition of DID curve is the change of dimensionless intensity variable by dimensionless time, it is possible to calculate rainfall duration, t_{r}, for the IDF graph through the following expressions:

$$t = t_{\mathrm{r}} t_{\mathrm{d}} \tag{2.28}$$

On the other hand, consideration of DID curve expression from Eq. (2.27) with the rainfall amounts, r_{e}, the intensity, i, is calculated as,

$$i = i_{\mathrm{i}} r_{\mathrm{e}} \tag{2.29}$$

6. The application of the previous steps to each one of the stations leads to IDF curves for each one of them.

2.13 Probably Maximum Precipitation (PMP)

The probable maximum precipitation (PMP) is necessary for calculating the probable maximum flood (PMF), which is necessary in many design water-related projects at a particular geographical location in a given drainage basin. It also provides information for designing the size (dam height and reservoir storage

capacity) of the given project. Furthermore, dimension of the flood-carrying structures (spillway and flood-carrying tunnel) is also dependent on the PMP and subsequent PMF. Storm rainfall events and their subsequent floods have physical upper limits, and they are referred to as PMP and PMF.

Among the water resource management features, the most significant satisfactions are for the needs of society and the economy in addition to the protection of water and the natural environments. In any drainage basin where the probable maximum flood (PMF) occurrences are important, the preliminary step is to calculate point-wise and regional PMP amounts. The PMF quantities are important, especially for dam planning, design, and operation works at a particular section of drainage basin mainstream line. In particular, in arid regions, the construction of surface dams for flood protection and groundwater recharge is bound to increase due to climate change impact, which indicates that in the future there will appear rainfall increments especially over the Arabian Peninsula. World Meteorological Organization, WMO (2009, 2011), defined the PMP as the theoretically greatest depth of rainfall that is physically possible in a given time interval (minute, hour, day, etc.) over a particular area and geographical location at a given time of the year.

Numerical determination of the PMP can be achieved by different methodologies depending on the availability of data. Among these scientific works are the ones due to Hansen et al. (1982), Foufoula-Georgiou (1989), BOM (1994), Collier and Hardaker (1996), Svensson and Rakhecha (1998), Corrigan et al. (1999), Desa et al. (2001), Rakhecha and Clark (2002), Rezacova et al. (2005), Papalexiou and Koutsoyiannis (2006), Desa and Rakhecha (2007), and Şen (2008). It is possible to consider the collection of these approaches into two categories, namely statistical analysis of rainfall frequency and genetic analysis based on synoptic situations, where vertical radio-zoning measurements are important for precipitable precipitation calculations (Sect. 2.16).

2.13.1 Definitions of PMP and PMF

Theoretically, PMP is the maximum precipitation for a given duration during which there are proper rainfall records that is assumed to be distributed over the whole drainage basin rather uniformly, or a storm area of a given size, at a certain time of year. Under a set of conditions and assumptions, PMP can be converted theoretically into PMF and it poses extremely serious threats to the flood control of a given project design. Such a flood could plausibly occur in a locality at a particular time of year under current meteorological conditions.

2.13.2 Statistical Estimates

The PMP amounts can be estimated approximately by the statistical approaches. The basis of such approaches is a frequency analysis with its two specific

properties, namely the arithmetic average and the standard deviation. The PMP statistical method concentrates on a wide region or a drainage basin by taking into account the individual station records available in the region. It helps to appreciate the upper physical limit of a storm. On the other hand, the statistical maxima are calculated according to the frequency analysis that corresponds to a certain risk level. The essence of the method is storm transposition, but instead of transposing the specific rainfall amount of one storm, the frequency factor, K, concept is adapted in almost all the water-related projects.

For the use of the PMP calculation, sufficient amount of data must be available, for instance, records of at least 30 years and also several stations scattered over the study area. In such an approach, the only meteorology data are precipitation records without any other meteorology variables. Figure 2.32 shows the change of K with the amount of mean annual maximum rainfall. These charts are useful for making quick decisions for drainage areas of less than 1000 km^2. One of the shortcoming of the procedure is that it yields point PMP, and therefore, it is necessary to apply area reduction calculation through convenient curves for adjusting the point values different size areas (see Fig. 2.28).

In the selection of appropriate frequency factor value, extreme value statistical PDF is necessary that is representative of the extreme values. A second problem is determining the appropriate value to use for K, which is a statistical variable that depends on the frequency distribution of extreme value hydrological data. According to the data at hand, different K values have been used by various investigators (Dhar and Damte 1969).

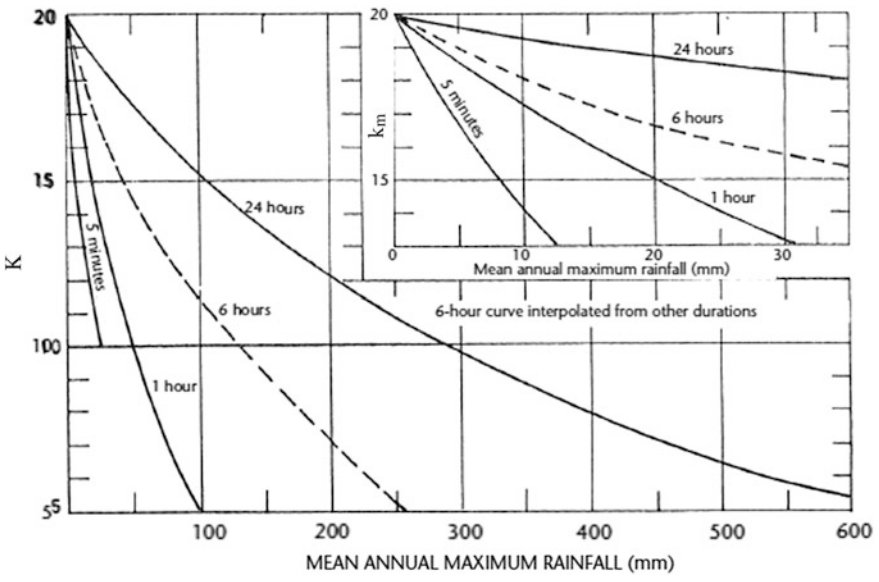

Fig. 2.28 K as a function of rainfall duration and mean of annual series (Hershfield 1965)

The procedure is suggested first by Hershfield (1961, 1965), and later, Hershfield (1965) modified it leading to a general frequency equation (Chow 1964).

$$X_T = \overline{X}_n + K\,S_n \tag{3.30}$$

where X_t is the rainfall for return period T, $\overline{X}_n$ and S_n, are, respectively, the mean and standard deviation of annual maximum precipitation records of length, n, and K is the frequency factor.

Extreme rainfall amounts of rare magnitude or occurrence are often found to have occurred at some time during a much shorter period of record, such as 30 years. Such a rare event is regarded as an outlier with an appreciable effect on the mean $\overline{X}_n$ and standard deviation S_n of the annual series. The effect is smaller (bigger) for long (short) records. Hershfield (1965) has studied this effect by using hypothetical series of varying lengths. Figures 2.29 and 2.30 indicate the necessary adjustments to be made on X_n and S_n in order to compensate for any outlier. In these figures, X_{n-m} and S_{n-m} refer to the mean and standard deviation of the annual maximum series after excluding the maximum item in the series. It should be noted that these relationships consider only the effect of the maximum observed event, but no consideration is given to other anomalous observations.

Increase in the record length may cause increase in the arithmetic average and the standard deviation of the annual maximum rainfall series. In general, the PDF of

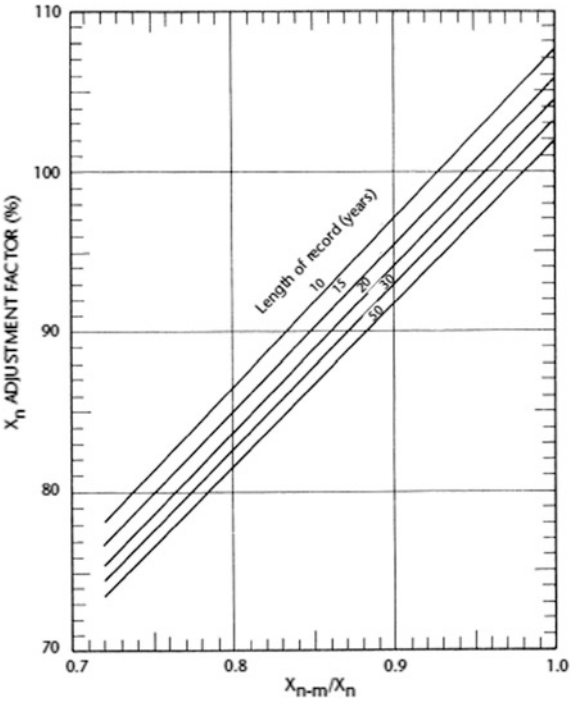

Fig. 2.29 Adjustment of mean of annual series for maximum observed rainfall (Hershfield 1965)

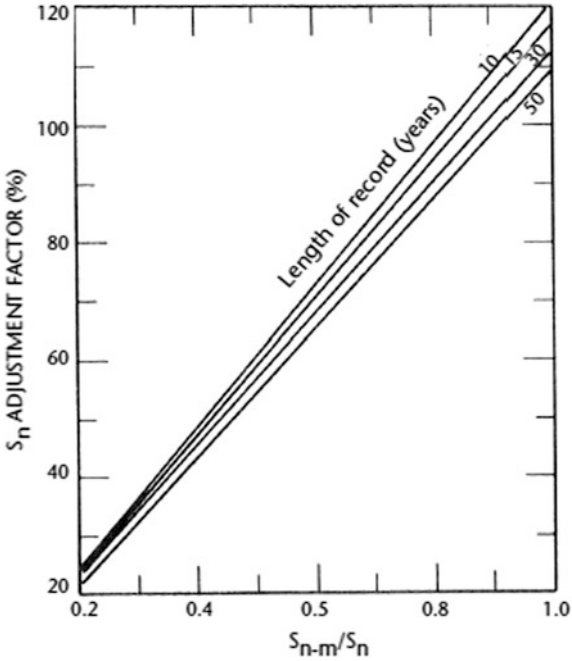

Fig. 2.30 Adjustment of standard deviation of annual series for maximum observed rainfall

rainfall extremes is skewed to the right and this provides greater opportunity for largeness than a small extreme as the length of record increases. Figure 2.31 provides a basis for adjustments in the mean and standard deviation according to the record length.

In general, the precipitation data are not recorded instantaneously, but over a certain time interval such as 6 hours, daily, weekly, monthly, or annually. Such data recording system hides actual maximum rainfall records. Maxima for longer duration are different to a certain extend than the maxima in a shorter duration record.

Studies of thousands of station-years of rainfall data indicate that multiplying the results of a frequency analysis of annual maximum rainfall amounts for a single fixed time interval of any duration from 1 to 24 h by 1.13 will yield values closely approximating those to be obtained from an analysis based on true maxima (Hershfield 1961). Hence, the PMP values yielded by the statistical procedure should be multiplied by 1.13, if data for single fixed time intervals are used in compiling the annual series. Lesser adjustments (Weiss 1964) are required when maximum observed amounts for various durations are determined from two or more fixed time intervals (Fig. 2.32). Thus, for example, maximum amounts for 6-hour and 24-hour periods determined from 6 and 24 consecutive 1-hour rainfall increments require adjustment by factors of only 1.02 and 1.01, respectively.

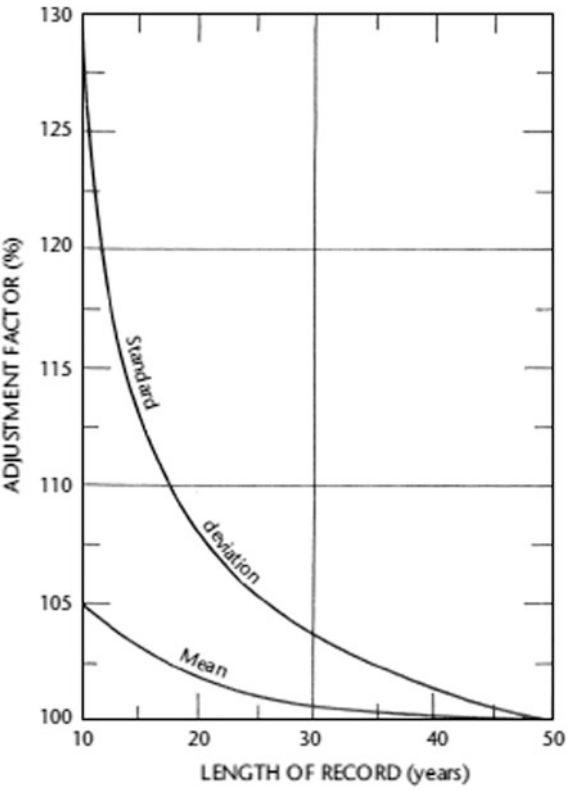

Fig. 2.31 Adjustment of mean and standard deviation of annual series for the length of record

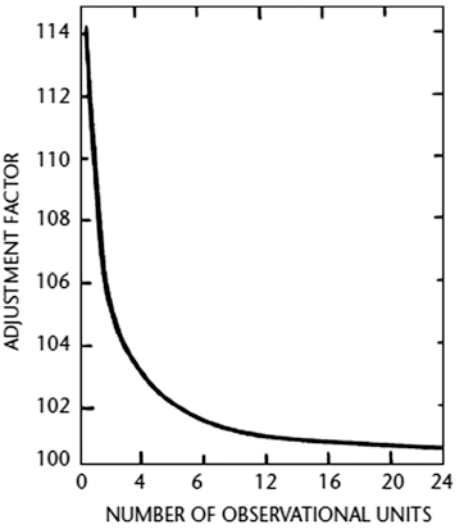

Fig. 2.32 Adjustment of fixed-interval precipitation amounts for number of observation units

2.13.3 Area Reduction Curves

The procedure that is valid for point rainfall data requires some other procedures for reduction of the point values to some required distances or areal rainfall averages. As mentioned by Miller et al. (1973), there are two types of depth–area relations. The first is the storm-centered relation, that is, the maximum precipitation occurring when the storm is centered on the area affected (Fig. 2.33a). The second type is the geographically fixed area relation, where the area is fixed and the storm is either centered on it or displaced so that only a portion of the storm affects the area (Fig. 2.33b). Storm-centered depth–area curves represent profiles of discrete storms, whereas the fixed area data are statistical averages in which the maximum point values frequently come from different storms.

The most convenient curves are the storm centers and surrounding ones for PMP studies. Court (1961) mentioned that there are different variations of depth–area relation curves (DAD). The relation in Fig. 2.34 is an idealized example, but similar curves must be developed for the study area. They will look alike to these curves as the study area enlarges the curves will decrease and curves should be developed for the specific location of the project.

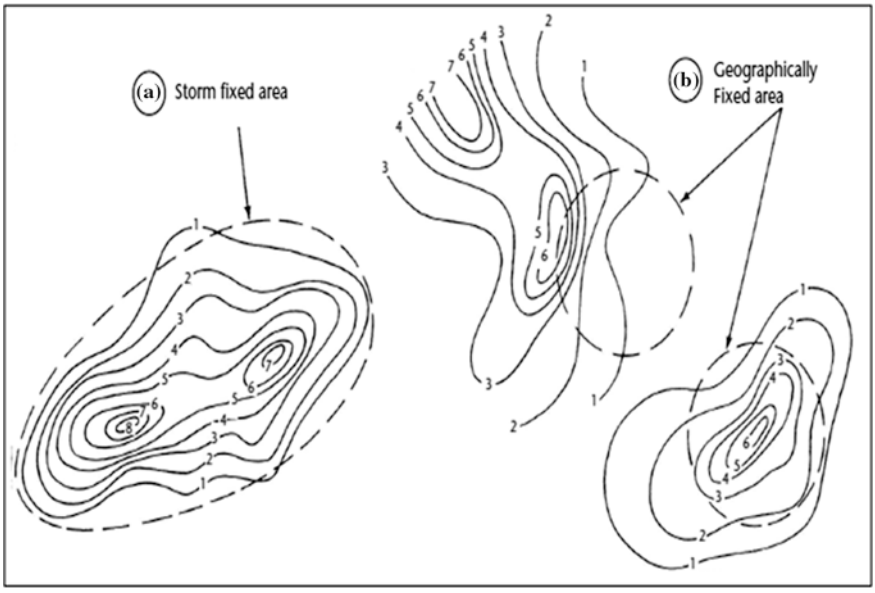

Fig. 2.33 Example of (**a**) isohyetal pattern centered over basin as would be the case for storm-centered depth-area curves and (**b**) two possible occurrences of isohyetal patterns over a geographically fixed area as would be the case in development of curves for a geographically fixed area (Miller et al. 1973)

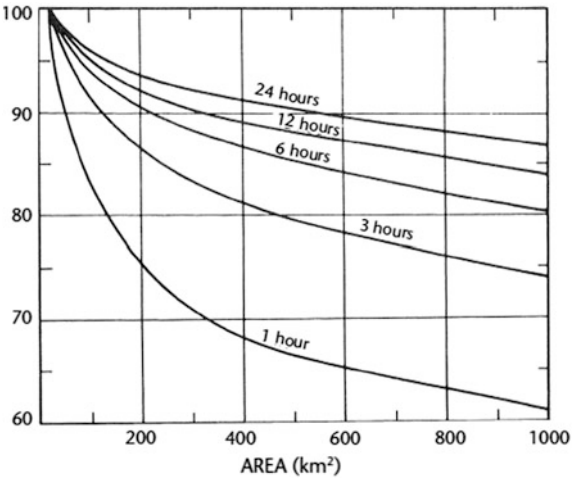

Fig. 2.34 Depth-area or area reduction curves for western USA (United States Weather Bureau 1960)

2.13.4 PMP and PMF Estimations

Thunderstorm rainfall events and consequent floods have upper physical level that cannot be transgressed theoretically. These limits are referred to as the PMP and PMF, respectively. Only their approximate estimations are possible in practical applications, because of the lack in hydrometeorological data sources, because of physical, meteorological, and hydrological complexities.

In the estimation the major factors are the precipitation intensity and efficiency as well as maximum moisture content between the surface and the cloud bases. The PMP estimation can be achieved through one of the two approaches. The first one is based on the PMPs estimations with different durations and areas. It provides a set of methods to convert them into the PMP in the design drainage basin for the purpose of PMF estimation for high-risk cases.

The other method based on drainage basin area is a direct approach, which focuses on the PMP estimation based on a given duration that is determined according to a specific project in the study area with comparatively lesser risk level. For instance, construction of a reservoir in the study area requires such an approach. The duration of the design flood is taken relatively long; the final design storm may be generated through the superposition, and it is the main controlling factor for the project regarding flood control. The required design flood duration may hence be shorter, and a storm may be generated by a single storm weather system or by local violent convection.

On the other hand, as for the PMF estimation, there are six different approaches that are currently used. These are as follows:

(a) The local storm maximization with an effective local model: In this approach, PMP is estimated on the basis of the maximum storm past observation in the study area. The application requires several years of meteorology data.

(b) The storm transposition model: Extraordinarily large storm is transported from the adjacent area to the study region. For this purpose, the probability of storm transposition is necessary, which can be obtained either by determination of meteorologically homogeneous zones over the study area or by a sequence of operations and modifications on the transposition storm so as to suit the local characteristics. It is widely used for design areas, where high-efficiency storms are rare.
(c) The temporal and spatial maximization of storm through a combination model: This model combines two or more storms that occurred over the study area on the basis of synoptic features of the region so as to obtain an artificial, but representative storm with a long duration. It is applicable for PMP and PMF estimations in large drainage basins with long durations, but requires strong meteorological knowledge.
(d) The theoretical inferential model: The basis is a three-dimensional storm structure that takes place over the study area and its conversion to a simple physical storm equation with the main physical factors effective in the study area. In the approach, either a laminar or a convergence model is used. The following points are significant in the convergence model.
(e) The generalized estimation model.
(f) The statistical estimation model.

These methodologies are usable mostly in medium-latitude or low-latitude areas. Their use in tropical low-latitude areas requires some parameters. Furthermore, additionally, the following two methods can also be used for deriving PMP and PMF estimations in extremely large drainage basins. It is assumed that the inflow of storm moisture converges to the center from all sides and rises to generate a storm event. However, in the case of laminar flow, it is assumed that the inflow of storm moisture crawls along an inclining surface in a laminar fashion and rises to generate an event. For the success of this method, upper layer meteorology data are necessary and it can be applied to very large areas.

(a) The major temporal and spatial combination and generalization method: It helps to estimate PMP over large and meteorologically homogeneous areas. The rainfalls are of orographic (elevation difference) type, and their convergence is toward an observed rainfall storm. This method has the results of PMP depth that show a generalized depth–area–duration (DAD) curve, spatial and temporal distribution of PMP.
(b) The storm simulation method based on the statistics historical floods: The PMP estimation is obtained by taking into account a set of numerous rainfall stations in a meteorologically homogeneous region, and the use of hydrological frequency analysis leads to generalized method. As explained by Wang (1984), the procedure is different from the traditional frequency analysis method.

2.13.5 Application of Procedure

The PMP calculation procedure can be found in the manual for estimation of probable maximum precipitation (WMO 2009) provided that long data series (more than 15 years) are available. The basis of the statistical PMP calculation methodology has been presented by considerations from the frequency equation by Hershfield (1965), which can be summarized as follows. In general, the PMP is a function of the arithmetic average of the daily maximum precipitation, $\overline{X}$, and the standard deviation, S_X, of the whole maximum daily rainfall time series through the factor, k_m, of the standard deviation as,

$$\text{PMP} = \overline{X} + k_m S_X \tag{2.31}$$

Herein, k_m is referred to as the frequency factor, which is a very important part of Eq. (2.31) as it constitutes the number of standard deviations added to the mean distribution value in order to attain the largest possible precipitation value within a series. If the annual number of maximum daily rainfall is n, then the exclusion of the maximum among the maxima daily rainfalls leads to another maximum daily rainfall series of length $n - 1$. For such a situation, the maximum daily rainfall amount can be related to the arithmetic average and the standard deviation of this new series similar to Eq. (2.31) as follows:

$$R_{\max} = \overline{X}_{n-1} + k_m S_{X(n-1)} \tag{2.32}$$

Hence,

$$k_m = \frac{R_{\max} - \overline{X}_{n-1}}{S_{X(n-1)}} \tag{2.33}$$

The internal structure of maximum daily rainfall amounts at each station is identified by the Gamma probability distribution function (PDF). Table 2.3 includes the statistical parameters and the PDF parameters.

The recorded data as well as the theoretical PDF are shown for each meteorology station. It is possible to calculate the maximum daily rainfall amount corresponding to a set of return periods as in Table 2.4, but none of these values are indication of the PMP. In this table, 2-, 5-, 10-, 25-, 50-, 100-, 250-, and 500-year return periods are given.

The PDF graphs provide a basis for the analysis of the frequency distribution of maximum daily rainfall mounts as well as their visual variability, and hence, numerical values include the median, the lower and upper quartiles (25 and 75%), the interquartile range, and extremes.

The basic values for the PMP numerical value calculations are given in the 3rd, 4th, 5th, and 6th columns in Table 2.5 according to Eqs. (2.31)–(2.33).

Table 2.3 Statistical parameters

Station number	Statistical parameter		Gamma PDF parameters	
	Mean (mm)	St. dev. (mm)	Alpha	Beta
J102	28.40	20.70	0.88	33.10
J113	46.66	35.51	2.23	21.00
J114	36.96	27.44	1.53	24.20
J134	28.81	25.40	1.27	22.70
J204	36.50	20.60	2.82	13.10
J205	36.50	20.59	1.90	23.10
J214	32.20	25.11	1.61	20.00
J219	23.75	20.83	1.29	18.50
J220	21.67	16.55	1.11	19.50
J221	27.51	27.62	1.31	21.00
J139	24.38	16.37	1.58	15.40
41024	28.94	22.74	1.26	23.00
Minimum	**7.10**	**5.34**	**0.53**	**4.96**
Average	**31.02**	**23.29**	**1.57**	**21.22**
Maximum	**46.66**	**35.51**	**2.82**	**33.10**
St. Dev.	**21.67**	**16.37**	**0.88**	**13.10**
Regional	*28.93*	*22.74*	*3.57*	*19.4*

Table 2.4 Maximum daily rainfall amounts

J102	22.68	43.69	58.45	77.26	91.16	104.88	122.78	136.21
J113	39.89	68.97	88.50	112.83	130.53	147.83	170.22	186.89
J114	29.27	57.07	76.69	101.33	120.33	138.66	162.62	180.59
J134	21.71	45.37	62.54	84.79	101.41	117.91	139.58	155.89
J204	32.28	52.45	65.65	81.85	93.52	104.86	119.46	130.27
J205	36.35	65.93	86.19	111.70	130.39	148.74	172.58	190.39
J214	25.84	49.43	65.95	86.97	102.49	117.79	137.77	152.74
J219	17.95	37.34	51.39	69.57	83.15	96.62	114.30	127.62
J220	15.63	34.56	48.61	67.01	80.86	94.65	112.84	126.56
J221	20.92	34.17	59.24	80.00	95.46	110.86	131.01	146.18
J239	19.48	37.50	50.15	66.27	78.19	89.95	105.31	116.81
41024	21.72	45.62	63.00	85.53	102.38	119.11	141.08	157.63
Minimum	**15.63**	**34.17**	**48.61**	**66.27**	**78.19**	**89.95**	**104.31**	**116.81**
Average	**25.31**	**47.68**	**65.00**	**85.43**	**100.82**	**115.99**	**135.80**	**150.64**
Maximum	**39.89**	**68.97**	**88.50**	**112.83**	**130.53**	**148.74**	**172.58**	**190.39**
St. Dev.	**7.59**	**11.64**	**13.14**	**15.85**	**17.94**	**20.00**	**22.73**	**24.81**
Regional	*62.84*	*96.63*	*118.22*	*144.39*	*163.08*	*181.11*	*204.20*	*221.23*

Table 2.5 PMP numerical values

Meteorology station	Record duration	Global parameters		Maximum exclusion parameters		Frequency factor	PMP (mm)	
		Mean (mm)	Standard deviation (mm)	Mean (mm)	Standard deviation (mm)		Past	Climate change
J102	1966–2011	28.40	20.70	26.30	16.06	4.22	151.00	173.65
J113	1966–2005	46.66	35.51	42.77	26.55	5.57	244.00	280.60
J114	1967–2013	36.96	27.44	33.69	23.86	2.73	112.06	128.87
J134	1970–2012	29.39	25.49	26.83	20.30	4.79	151.35	174.05
J204	1966–2005	36.50	20.60	35.10	18.91	2.88	95.87	110.25
J205	1966–2005	43.76	26.77	41.87	24.27	3.11	127.06	146.19
J214	1966–2006	32.20	25.10	30.02	20.99	4.37	141.99	163.29
J219	1970–2006	23.75	20.83	22.14	18.97	2.80	82.01	94.31
J220	1966–2011	21.67	16.55	20.57	15.08	3.13	73.50	84.53
J221	1971–2006	27.51	27.62	23.62	17.91	6.51	207.25	238.34
J239	1976–2011	24.38	16.37	23.24	15.34	2.30	62.10	71.41
41024	1970–2009	28.94	22.74	27.25	20.89	2.67	89.61	103.05

The application of Eq. (2.33) with the arithmetic mean and standard deviation values in columns 5 and 6 yields the frequency factor values in column 7. Table 2.5 indicates that the frequency factor values vary between 2.30 and 6.51. The same table indicates that one-day past PMP is the biggest (244 mm) at station J113 among other stations. Accordingly, the same is valid for the climate change effective calculations. There is a logarithmic relationship between the PMP and its corresponding frequency factor as in Fig. 2.35.

The logarithmic relationship between the PMP and the frequency factor is given as follows:

$$\text{PMP} = 70k^{0.757} \tag{2.34}$$

Although this expression represents past and climate change PMP values, one can construct another straight line on this graph just for the climate change effects and it will be shifted upward slightly. This task is left outside the work in this book, because it is not necessary for the completion of the study.

Figure 2.36 shows the frequency factor distribution with the meteorological station. The arithmetic mean and the standard deviation of the frequency factor are 3.76 and 1.33, respectively.

The maximum and minimum frequency factors are at the J221 and J239 meteorology stations, respectively. For a regional assessment, one can use the arithmetic average of the frequency factor, which is equal to 3.76; however, such a work is not necessary for this section, because the regionalism is worked with the maximum daily rainfall amounts irrespective of the meteorology stations as shown in the last row in Table 2.4. Figure 2.37 indicates the change of annual maximum daily rainfall pattern in the study area.

The correspondence to the annual maximum rainfall time series is the PDF according to the Gamma function with the relevant parameters as in Fig. 2.38. Although the PMP ($\sim$145 mm) is the greatest than any other station (point-wise)-based amounts, in this section it will not be used, because the climate change PMP

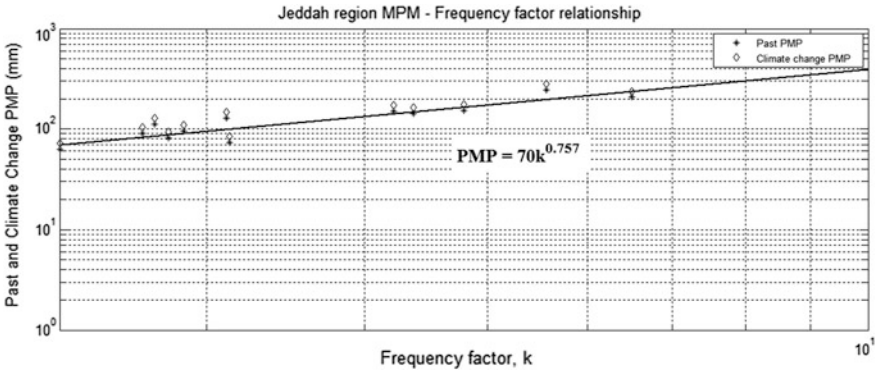

Fig. 2.35 PMP–frequency factor relationship

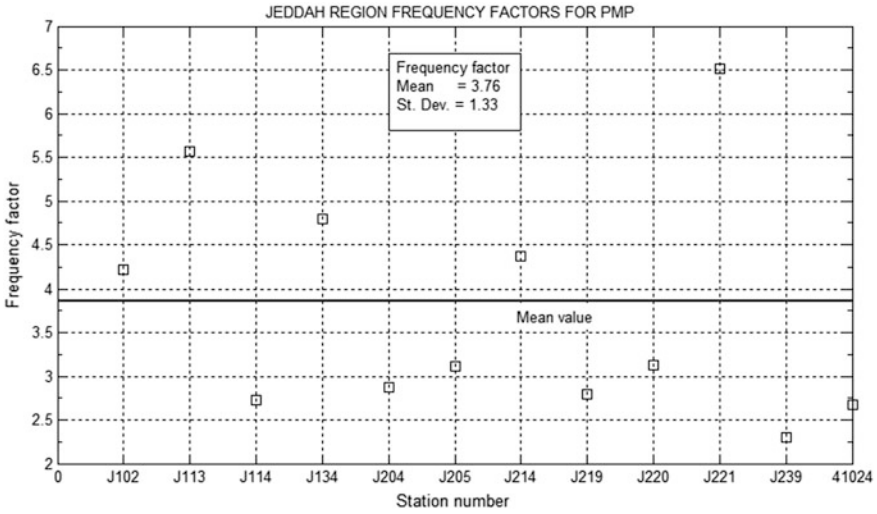

Fig. 2.36 Frequency factor distributions with meteorology stations

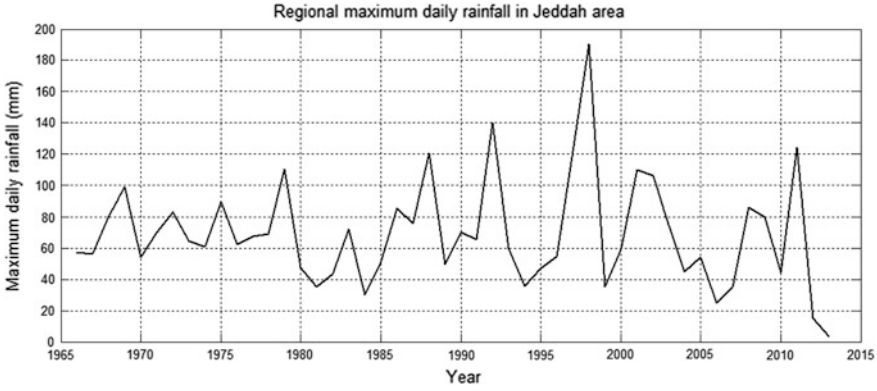

Fig. 2.37 Annual maximum daily rainfall time series

map indicates that the dam locations are close to the coastal area, where the spatial variations are rather smaller.

Figure 2.39 shows the change of PMP along the meteorology stations both for past records and for climate change projections.

This relationship can be regarded as the regional expression for the PMP calculation in the Jeddah area. Out of 12 stations, seven (J102, J113, J114, J134, J205, J214, and J221) have PMP values more than 100 mm on the basis of past record bases. Climate change effect increases this number to nine stations including J204 and 41024. Relatively low maximum daily rainfall amounts, especially those smaller than 100 mm, are observed at meteorology stations J219, J220, and J239.

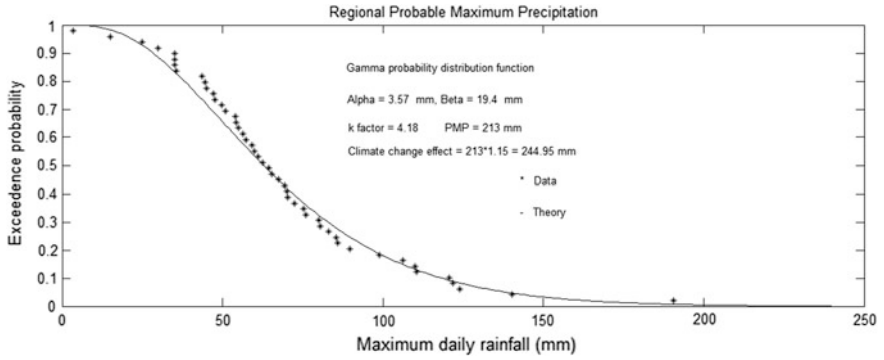

Fig. 2.38 Annual maximum daily rainfall characteristics

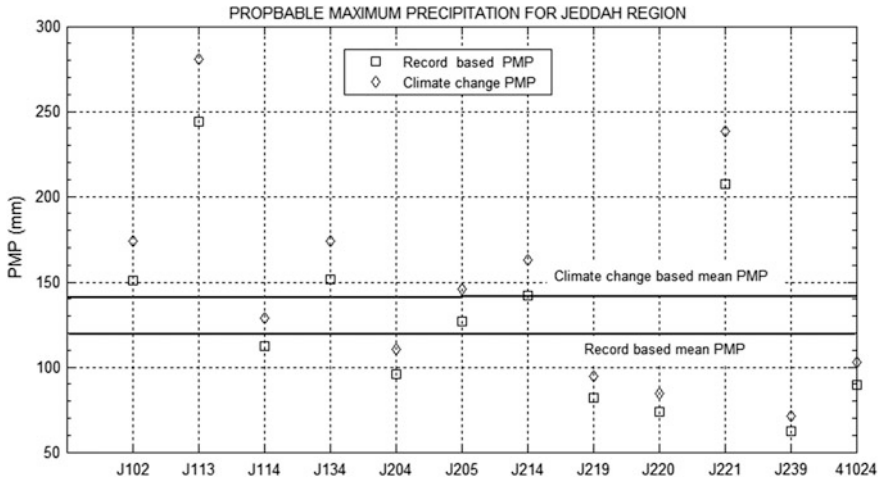

Fig. 2.39 PMP change along stations

On the other hand, storm cells are observed at the time, which resulted in extremely high rainfall levels at stations other than those included in the analysis. While the long-term annual average rainfall for Jeddah City is approximately 55 mm, the Saudi Geological Survey (SGS) has estimated that some 160 mm of rainfall fell on November 25, 2009, for the duration of about 3 h, leading to the disastrous consequences. It is obvious from Table 6.7 that the first three maximum daily rainfall records have been observed at J113 (190.6 mm), J221 (140.2 mm), and J205 (117.4 mm) stations. The maximum rainfall amounts are related to the movement of moist westerly or northwesterly fronts or large areas of low pressures. Additionally, another potential reason is due to the fact of the hot flow and humid tropical air from the Red Sea region and its convergence with polar marine air over the study area.

Table 2.6 Rainfall efficiency

Years	Stations											
	J102	J113	J114	J134	J204	J205	J214	J219	J220	J221	J239	41024
R_{max}	110.5	190.6	99	124	89.6	117.4	121.8	75.2	67.8	140.2	58.6	83
PMP (past)	151	224	112.1	151.4	95.9	127.1	142	82.01	73.5	207.3	62.1	89.6
PMP (climate)	173.7	280.6	128.9	174.1	110.3	146.2	163.3	94.3	84.6	238.3	71.4	103.1
Efficiency (past)	1.37	1.18	1.13	1.22	1.07	1.08	1.17	1.09	1.08	1.48	1.06	1.08
Efficiency (climate)	1.57	1.47	1.30	1.40	1.23	1.25	1.34	1.25	1.24	1.70	1.22	1.24

2.13.5.1 Efficiency Factor

In order to see how close are the actually recorded maximum daily rainfall amounts to the calculated PMP values, the efficiency factor, E, can be defined as the ratio of the calculated past and climate effective PMPs to the maximum daily rainfall, R_{max}.

$$E = \frac{\text{PMP}}{R_{max}} \tag{2.35}$$

The sixth and seventh rows in Table 2.6 are the efficiency values, which are always more than one. It implies that in the study region yet the PMP values are not reached by the recorded rainfall occurrences, and hence, there is still room for more dangerous rainfall occurrences. At places, the difference is more than 70%. This point implies that for future designs concerning any engineering structure (dams, diversion canals, roads, etc.) need more care and to be on safe side, these structures must be constructed based on the PMP values.

2.13.5.2 Regional Variations

In order to appreciate the regional variation of the frequency factor and the PMP amounts for past and climate change contribution cases maps are prepared and shown in Figs. 2.40, 2.41, and 2.42. Each one provides visual inspection of regional variations around the Jeddah area, and one can then decide which PMP values to adopt for the PMF calculations for this region as explained in the next section.

This figure shows that close to the area of dams (within the study area), the PMP frequency factors vary from 3.2 to 4.6 in the north–south direction. In the PMF calculations, it is recommended that the contours within the study area encircled by the pink line should be taken into consideration in any further calculations.

Within the study area, the past PMP contours have values between 110 mm and 170 mm with the lowest one around the Jeddah Airport meteorology station number with 41024.

This figure has almost the same pattern as the past PMP pattern in Fig. 2.41, but comparatively with bigger values. In the future calculations, these contour values must be considered, because it has the effects of the past records and the climate change impact.

2.14 Probable Maximum Flood (PMF)

The estimation accuracy of PMP/PMF is dependent on the quantity and quality of data, especially on the extraordinary storms and floods. Even then it is not possible to say that their estimations are precise, because there is no a complete methodology

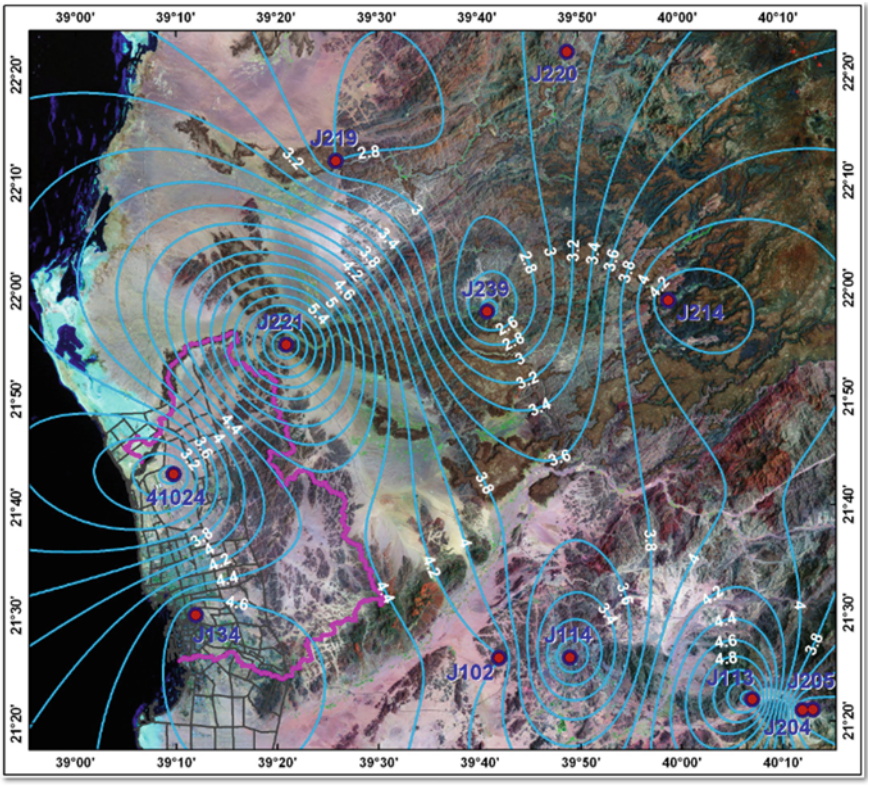

Fig. 2.40 Frequency factor regional distributions

for this purpose. It is necessary to analyze, compare, and harmonize estimation results from a set of different methods. For the quality control, various methodological results can be compared and, if necessary, their ensemble averages can be taken in some manner. In the comparison studies, it is necessary to care for the amount by which the PMP estimation exceeds the maximum rainfall record values for the adjacent meteorologically homogeneous region. Additionally, the frequency and severity of storms records should be taken into consideration. There may be limitations in the storm transposition in the region. Furthermore, the reliability of relations between rainfalls and other meteorological variables is also important for the comparison purposes.

After the completion of the PMP calculations, it is now time to convert the values through a convenient rainfall–runoff relationship so as to calculate the peak discharges and the resulting hydrographs. It is, therefore, necessary to calculate the duration of the rainfall within a day. This can be achieved empirically according to the Snyder method (Chap. 5), which gives the time to peak discharge by taking into consideration the longest channel length, L, and the length of this channel from the projection of the centroid point on the channel and the outlet, L_c, in addition to the slope value.

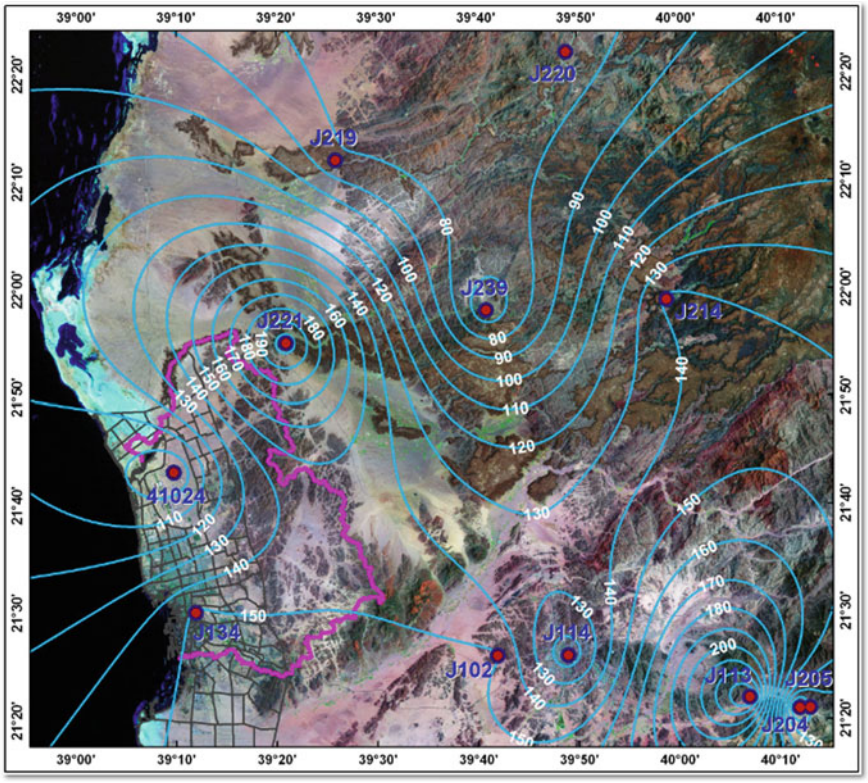

Fig. 2.41 Past PMP regional distributions

The peak discharge values can be calculated according to various methodologies such as the Snyder, SCS, kinematic wave, and other methodologies (Şen 2008). However, in this section, the simplest one is considered according to the rational approach, which can be used with confidence especially in small drainage areas (Chap. 5).

For the PMF calculations, the catchments in the area are identified with their geomorphological features including the drainage area, main channel length, centroid length, and if necessary also the slope. The locations of 15 drainage basins that are the subject of this report are given in Fig. 2.43.

Table 2.7 includes the names and codes of the dams and also the names of wadis (drainage area) and sub-basins.

Table 2.8 includes all the necessary geomorphological features that will enter into the PMF calculations.

The execution of the three steps mentioned at the beginning of this section leads to the numerical results as shown in Table 2.9 (Figs. 2.44 and 2.45).

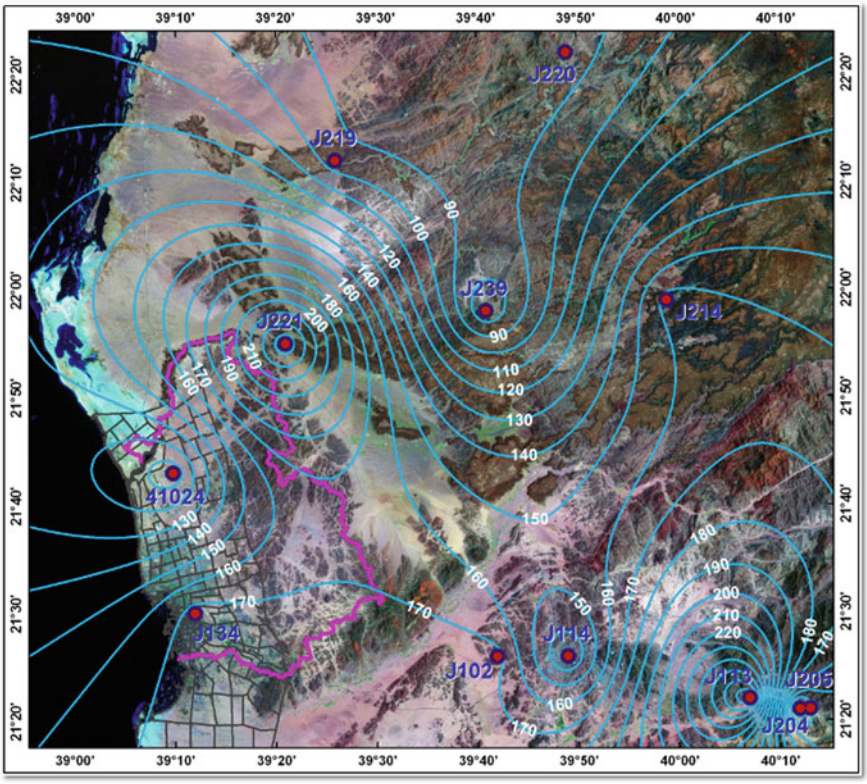

Fig. 2.42 Climate change PMP regional distributions

2.15 Precipitable Water Calculation

In this section, useful knowledge and information are presented by making use of the moisture content of the lower atmosphere between the Earth surface and the cloud bases. This type of calculation leads to another version of the PMP calculation and a set of verbal information deductions, especially those that are useful for analytical methodological developments.

The moisture content in the air can be converted to precipitable water amount by simple engineering approaches. The first modeling design is given in Fig. 2.46 in the form of a prism, where the horizontal base area is equal to 1 and the height as small as possible, dz.

In this air column, the conversion of the humidity into rainfall is referred to as the PMP. For PMP calculation, it is necessary to know the vertical variations of meteorological factors that cause to rainfall as temperature, T, pressure, p, and humidity, q. These factors vary temporarily and spatially. The vertical variations can be obtained from the radiosonde measurements. This leads to the vertical variation of humidity and pressure as in Fig. 2.47.

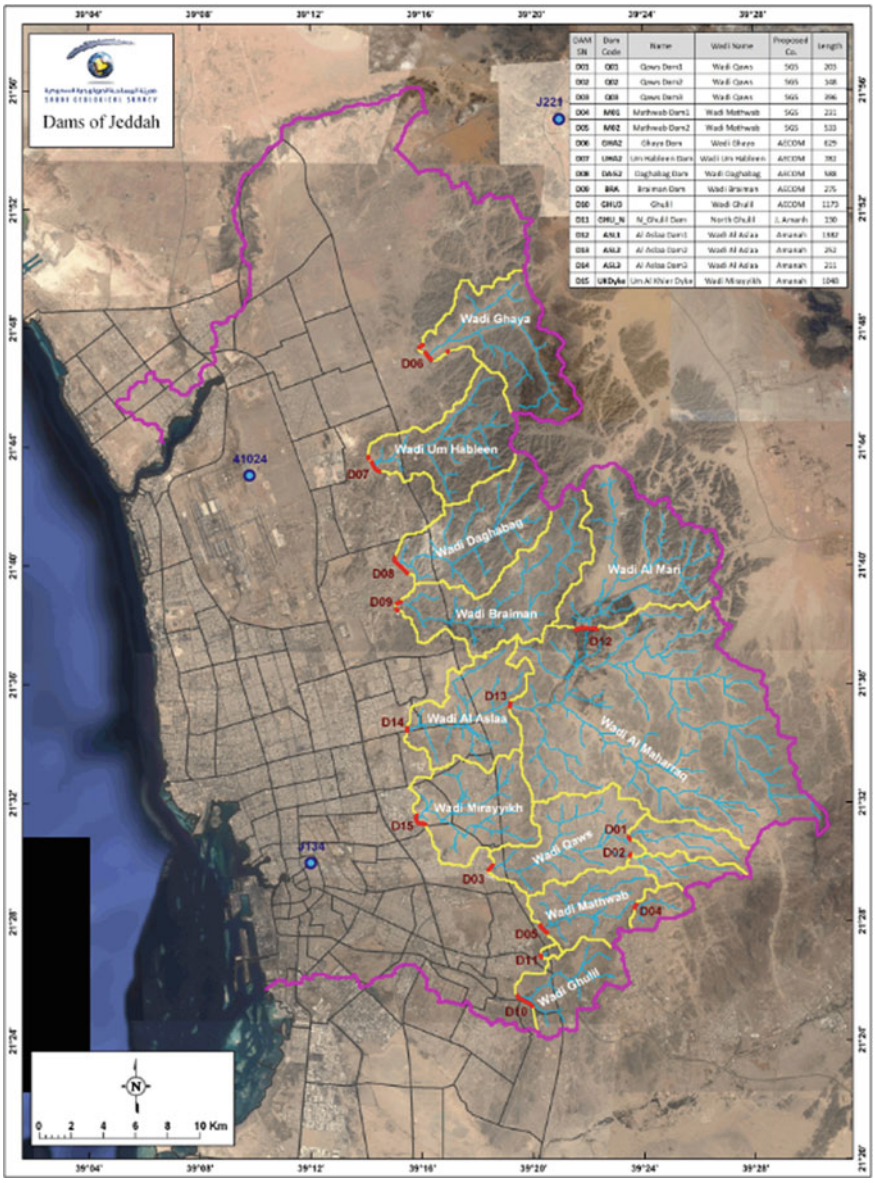

Fig. 2.43 Drainage area and dam locations

The specific humidity is defined as the ratio of water vapor density to air density, and it is a dimensionless quantity, but in practical applications, it is expressed as gr/kg. Based on the prism as in Fig. 2.46, if the water amount in dz height is ds, from the base to a height, h, the water amount variation is $s(h)$; provided that the water vapor density is ρ_s, then one can write that,

Table 2.7 Wadi names and dam codes

Dam SN	Dam Code	Name	Wadi Name
D01	Q01	Qaws Dam1	Wadi Qaws
D02	Q02	Qaws Dam2	Wadi Qaws
D03	Q03	Qaws Dam3	Wadi Qaws
D04	M01	Mathwab Dam1	Wadi Mathwab
D05	M02	Mathwab Dam2	Wadi Mathwab
D06	GHA2	Ghaya Dam	Wadi Ghaya
D07	UHA2	Um Hableen Dam	Wadi Um Hableen
D08	DAG2	Daghabag Dam	Wadi Daghabag
D09	BRA	Braiman Dam	Wadi Braiman
D10	GHU3	Ghulil	Wadi Ghulil
D11	GHU_N	N_Ghulil Dam	North Ghulil
D12	ASL1	Al Aslaa Dam1	Wadi Al Aslaa
D13	ASL2	Al Aslaa Dam2	Wadi Al Aslaa
D14	ASL3	Al Aslaa Dam3	Wadi Al Aslaa
D15	UKDyke	Um Al Khier Dyke	Wadi Mirayyikh

Table 2.8 Jeddah region drainage basins characteristics

Basin SN	Basin name	Wadi name	Area (km^2)	Basin slope (m/m)	MFDIST (m)	MFDSLOPE (m/m)	Centroid (m)
1	Qaws01	Wadi Qaws	14.247	0.02215	9519.2	0.0117	4424.5
2	Qaws02	Wadi Qaws	9.408	0.02277	8855.9	0.01244	3941.8
3	Qaws03	Wadi Qaws	38.291	0.03341	12098.6	0.00933	6092.7
4	Mathwab01	Wadi Mathwab	7.062	0.04009	4427.5	0.01097	1896.4
5	Mathwab02	Wadi Mathwab	26.492	0.03599	9087.2	0.00913	3802.9
6	Ghaya	Wadi Ghaya	46.087	0.10729	15239.6	0.0246	6449.8
7	Um Hableen	Wadi Um Hableen	39.672	0.11069	11419.7	0.03552	5780.4
8	Daghabag	Wadi Daghabag	46.269	0.10712	13892.3	0.02622	6844.4
9	Braiman	Wadi Braiman	51.269	0.056	20495.2	0.00932	9874.1
10	Ghulil	Wadi Ghulil	23.828	0.04337	8951	0.01139	4218.3
11	N_Ghulil		0.856	0.09268	1682.5	0.0436	477

(continued)

Table 2.8 (continued)

Basin SN	Basin name	Wadi name	Area (km^2)	Basin slope (m/m)	MFDIST (m)	MFDSLOPE (m/m)	Centroid (m)
		Wadi N_Ghulil					
12	Al Mari	Wadi Al Mari	62.601	0.05348	13022.6	0.00657	6998.8
13	Al Maharraq	Wadi Al Maharraq	188.261	0.03544	30974.4	0.01805	13099.6
14	Al Aslaa	Wadi Al Aslaa	37.54	0.06054	12596.7	0.0077	4611.4
15	Mirayyikh	Wadi Mirayyikh	38.373	0.04406	10313.2	0.01105	4723.6

Table 2.9 Jeddah region drainage basin parameters

Basin name	Wadi name	Area (km^2)	MFDIST (m)	CENTOUT (m)	Snyder tp (h)	Rational discharge (m^3/day)	PMF discharge (m^3/s)
Qaws01	Wadi Qaws	14.247	9519.2	4424.5	3.77	18837.98	62.33
Qaws02	Wadi Qaws	9.408	8855.9	3941.8	3.57	11758.44	43.54
Qaws03	Wadi Qaws	38.291	12098.6	6092.7	4.47	59886.95	141.63
Mathwab01	Wadi Mathwab	7.062	4427.5	1896.4	2.33	5756.03	50.12
Mathwab02	Wadi Mathwab	26.492	9087.2	3802.9	3.56	33010.41	122.99
Ghaya	Wadi Ghaya	46.087	15239.6	6449.8	4.87	78579.23	170.16
Um Hableen	Wadi Um Hableen	39.672	11419.7	5780.4	4.32	60026.18	124.91
Daghabag	Wadi Daghabag	46.269	13892.3	6844.4	4.82	78108.16	139.90
Braiman	Wadi Braiman	51.269	20495.2	9874.1	6.05	108560.73	131.82
Ghulil	Wadi Ghulil	23.828	8951.0	4218.3	3.66	30490.44	107.72
N_Ghulil	Wadi N_Ghulil	0.856	1682.5	477.0	1.15	344.96	12.29
Al Mari	Wadi Al Mari	62.601	13022.6	6998.8	4.76	104344.85	204.48
Al Maharraq	Wadi Al Maharraq	188.261	30974.4	13099.6	7.45	491147.66	392.88

(continued)

Table 2.9 (continued)

Basin name	Wadi name	Area (km^2)	MFDIST (m)	CENTOUT (m)	Snyder tp (h)	Rational discharge (m^3/day)	PMF discharge (m^3/s)
Al Aslaa	Wadi Al Aslaa	37.54	12596.7	4611.4	4.16	54663.26	140.36
Mirayyikh	Wadi Mirayyikh	38.373	10313.2	4723.6	3.94	53002.70	155.98

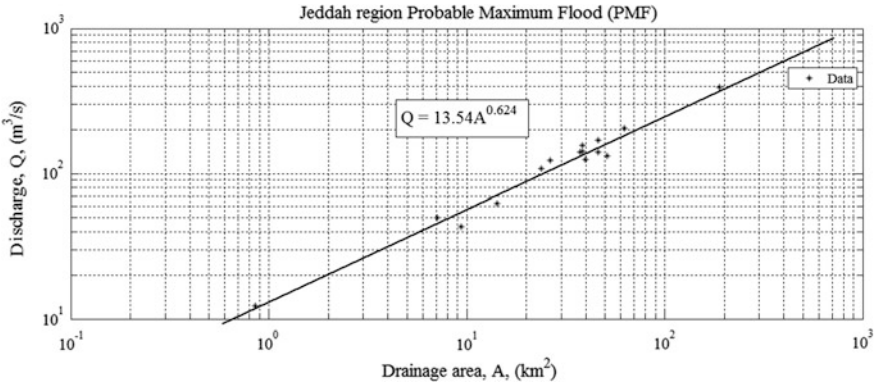

Fig. 2.44 Discharge–drainage area relationships

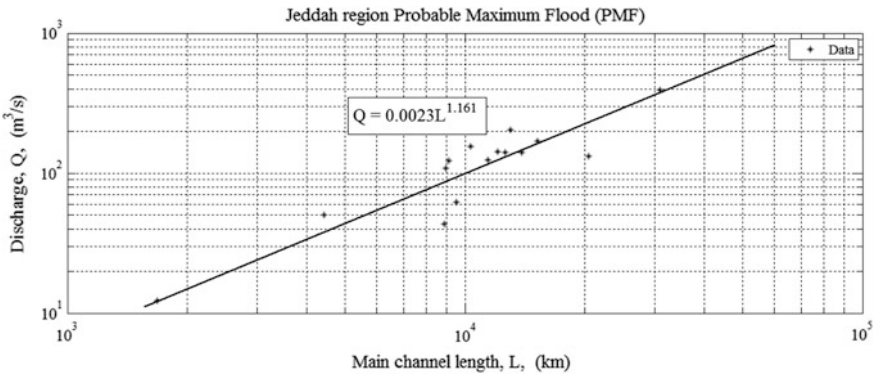

Fig. 2.45 Discharge–main channel length relationships

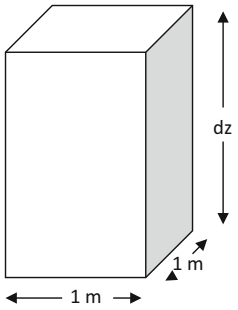

Fig. 2.46 Unit base area prisms

$$s(h) = \int_0^h \mathrm{d}s = \int_0^h \rho_s \mathrm{d}z \tag{2.36}$$

Instead of height, if pressure is considered then the hydrostatic equilibrium equation says that $\mathrm{d}p = -\rho_{\mathrm{H}} g \mathrm{d}z$. The subject of dz from this expression can be substituted into previous equation after the necessary arrangements leading to,

$$s(p) = -\frac{1}{\rho g} \int_{p_1}^{p_2} q \mathrm{d}p \tag{2.37}$$

where $q = \rho_{\mathrm{w}}/\rho_{\mathrm{H}}$ is the specific humidity; p_1 and p_2 are low and high-pressure levels, respectively. It is possible to render this expression into a more practical form by taking into account the g value approximately as,

$$s(p, q) = 0.0001 \int_{p_1}^{p_2} q \mathrm{d}p \tag{2.38}$$

This expression is useful to calculate the PMP precipitable water amount of the unit area base prism provided that the pressure variations between two levels (p_1 and p_2) are known. As shown in Fig. 2.47 from the radiosonde data, the determination of the specific humidity by pressure, the integration in Eq. (2.38) can be achieved and it shows the area of pressure change between two pressure levels. The multiplication of this area by 0.0001 leads to PMP amount. In order to obtain the rainfall height in cm, the specific humidity must be in gr/kg and the pressure in minibar.

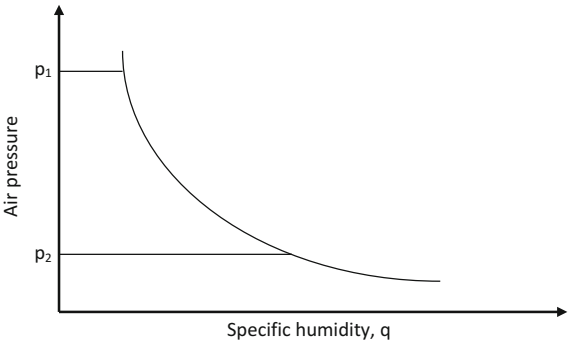

Fig. 2.47 Vertical humidity variations

2.15.1 Application Principles

In practical applications, in order to depend on easily applicable procedure instead of pressure consideration, water vapor density, ρ_{wv}, one can obtain the precipitable water volume, dV, within the unit area and dz height volume as,

$$dV = \rho_{wv} dz$$

Its integration from the earth surface to height h yields,

$$P(h) = \int_0^h \rho_{sp} dz \tag{2.39}$$

In these calculations, the humidity distribution, m, around the radiosonde trace is assumed to be constant. Precipitation in gram can be calculated by taking into consideration the absolute humidity measurement in gr/cm^3 as,

$$V(h) = \int_0^h m dz \tag{2.40}$$

In radiosonde measurements, the relative humidity, $m_{r,}$ records are obtained in percentage. For this reason, the relationships between the absolute and relative humidity are necessary in the applications. In this relationship, saturated water vapor,ρ_{swv}, is considered, and hence,

$$m_r = 100 \frac{\rho_{wv}}{\rho_{swv}} \tag{2.41}$$

Table 2.10 Dew point temperature and saturation water vapor density

T_d	ρ_{swv}
0	4.86
5	6.81
10	9.41
15	12.83

and

$$\rho_{swv} = \frac{m_r \rho_{swv}}{100} \tag{2.42}$$

The substitution of this expression into Eq. (2.39) yields,

$$V(h) = \int_0^h \frac{m_r \rho_{swv}}{100} dz \tag{2.43}$$

Herein, ρ_{swv} is a function of the saturation point temperature, T_s. The relationship between the two variables is given in Table 2.10.

The fit curve to these data gives the following expression:

$$\rho_{swv} = 5.0\, e^{0.0614\, T_s} \tag{2.44}$$

The integration Eq. (2.43) can be taken practically by finite difference approach as,

$$V(h) \cong \frac{\rho_{swv}}{100} \sum_{i=1}^{n} (m_r \Delta z)_i \tag{2.45}$$

2.16 Areal Average Rainfall Calculation

Rainfall records at individual meteorology stations represent the station vicinity rainfall amounts. However, in case of several meteorology station existence in an area, it is necessary to find the areal average rainfall (AAR) amount to know the rainfall amounts at any point within the study area. For the AAR calculations, there are various practical methods and in practical applications it is necessary to decide which one to use. In the following subsections, four of these methodologies are explained briefly, because they are available in any textbook on the hydrometeorology.

2.16.1 Arithmetic Average

This method yields plausible AAR values provided that the rainfall amounts at each station are not different more than 10% relative error percentage (Sect. 2.8.1). This means that there is more or less uniformly distributed areal rainfall prevalence over the study area. In order to check the 10% error percentage, e, it is necessary to pinpoint the maximum, R_{max}, and minimum, R_{min}, rainfall records among n number of stations by taking into consideration Eq. (2.2). Provided that $\alpha < 10\%$, then the AAR, $\overline{R}_A$, can be calculated according to the arithmetic average formula as,

$$\overline{R}_A = \frac{1}{n}\sum_{i=1}^{n} R_i \tag{2.46}$$

where R_i is the amount of rainfall at station i. It is important to notice that this expression is a special case of the following section rainfall calculation with equal weightings.

2.16.2 Weighted Average

This method considers for each station a certain portion of the drainage basin area, and accordingly, each rainfall station record is considered as effective over such sub-areas. In practical applications, these sub-areas are determined as polygons or percentage polygons.

2.16.2.1 Thiessen Polygon

Logically, each rainfall recorded at a raingauge should have its areal domain of influence, i.e., a representative sub-area. If the relative differences between the stations are more than 10%, then in the calculation of AAR, the role of representative sub-areas must be taken into consideration. It is not always clear how to get the most representative sub-area value. Although the advent of Geographic Information Systems (GIS) has greatly streamlined the problem of determining spatial statistics, sometimes it is not practical to use GIS; instead, Theissen (1912) polygon approach is probably the most common method used in hydrometeorology for determining AAR when there are several raingauge records. The basic concept is to divide the drainage basin into several polygons, each one around a measurement point, and then take the weighted average of the measurements based on the size of each polygon area.

The construction of sub-area polygons can be achieved as follows. Consider the drainage basin boundary as in Fig. 2.48 There is three raingauges inside the drainage basin, and the fourth is outside.

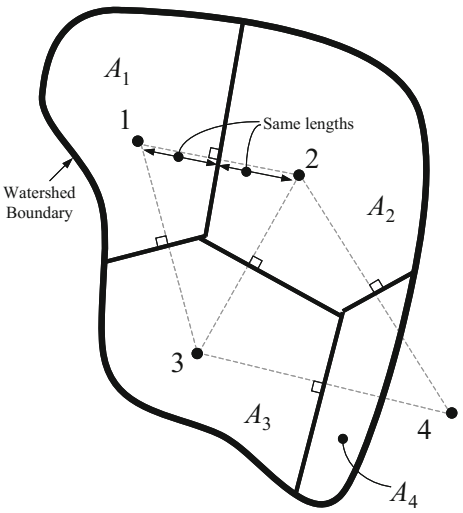

Fig. 2.48 Theissen polygonal divisions

The application of the Theissen areal weighting method first consists of constructing a series of triangles by joining pairs of adjacent rainfall stations. The nearest stations should always be jointed, and each triangle is kept near the equiangular shape when possible.

1. First connect all of the measurement points, the dots in the figure are measurement points, and they have been connected with dashed lines.
2. Draw perpendicularly bisect each of the "connecting" lines and extend the bisecting lines until either intersect the watershed boundary or another bisecting line.
3. Hence, four polygons are generated and note that measurements made at point 4 will contribute less to the final average than, say, the measurements at point 2.

If there are n stations, then there are n polygons and n representative sub-areas, A_i, for each station with the rainfall record, R_i. Provided that the representative polygons are decided, then the AAR can be calculated according to the following weighted average:

$$\overline{R}_{\mathrm{A}} = \frac{\sum_{i=1}^{n} R_i A_i}{\sum_{i=1}^{n} A_i} = \frac{1}{A}\sum_{i=1}^{n} R_i A_i = \sum_{i=1}^{n} R_i \frac{A_i}{A} = \sum_{i=1}^{n} R_i a_i \tag{2.47}$$

where a_i's are the percentage representative areas, and therefore, $0 < a_i < 1$ and $a_1 + a_2 + \ldots a_n = 1$. If the representative polygon sub-areas are all equal and amount to A_s, then $A_i/A = A_s/nA_s = 1/n$, and hence, Eq. (2.47) becomes equivalent to Eq. (2.46), which is the arithmetic average AAR calculation.

2.16.2.2 Şen Polygon

The major drawback in the Theissen polygon approach is that whatever the rainfall amounts, the sub-area polygons remain the same. These polygons are dependent entirely on the raingauge location configuration. Sometimes, it is possible that a very small rainfall at one of the stations may have a very big sub-area, and hence, the contribution may be more than another station, where the rainfall is much higher. In order to alleviate this drawback, Şen (1998) suggested that the representative sub-area polygons should not be dependent on the station configuration only, but in the meantime on the amount of the rainfall recorded at each station. This is the percentage-weighted polygon (PWP) method, which has the same basic triangularization procedure as in the Theissen polygon method.

After deciding on the triangles, the following procedure is necessary for dividing the study area into polygons leading to the PWP. If the rainfall values at three apices of a triangle are A, B, and C, then their respective percentages are calculated simply as,

$$pA = 100A/(A+B+C) \tag{2.48}$$

$$pB = 100B/(A+B+C) \tag{2.49}$$

and

$$pC = 100C/(A+B+C) \tag{2.50}$$

respectively. Hence, it is possible to find the three-variable percentage data of constant sums for each triangle. A two-dimensional plot of three variables can be shown on a triangular graph paper as one point (see Fig. 2.49). Such papers are very common tools in earth sciences (Koch and Link 1971).

In order to demonstrate the method more explicitly, the following step-by-step algorithm is provided:

1. Draw lines between each adjacent pair of rainfall stations. Hence, a set of triangles is obtained that cover the study area.
2. For each triangle, calculate the rainfall percentage at its apices according to Eqs. (2.48)–(2.50). Consider in each station that each apex has the value of 100 percentages with zero percentage on the opposite side.

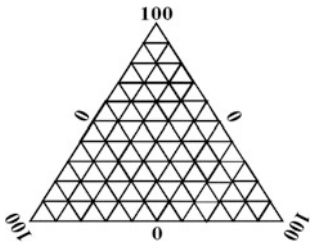

Fig. 2.49 Triangular coordinate paper

3. Consider bisector, which connects an apex to the midpoint of the opposite side and graduate it into 100 equal pieces.
4. By making use of one rainfall percentage calculation in step 2, mark it along the convenient bisector starting from the opposite side toward the apex.
5. Draw a parallel line from this marked point in step 4 to the opposite side of the apex considered with its rainfall percentage.
6. Repeat steps 4 and 5 for the next rainfall percentage and find similar parallel line this time to another opposite side.
7. The intersection of these two lines defines the key point for the triangle considered.
8. In order to check the correctness of this key point, repeat steps 4 and 5 for the remaining third rainfall percentage value. If the parallel line to the side crosses through the aforementioned key point, then the procedure of finding the key point for the triangle is complete. Otherwise, there is a mistake either in rainfall percentage calculations or in the location of marked points along the bisectors in steps 3 through 6 inclusive.
9. Return to step 2 and repeat the process for other triangles constructed in step 1. In this manner, each triangle will have its key point. The location of this point within the triangle depends on the percentages of recorded rainfall amounts at the three adjacent apices. The greater the rainfall percentage for an apex, the closer the point will lie to this apex. It is not necessary that the triangles resulting from a given set of stations in a network should be exactly equilateral. However, in the Theissen method for an obtuse-angle triangle, the intersection of the three perpendicular bisectors occurs outside the triangular area.
10. Key points at adjacent triangles are connected with each other to form polygons each including a single rainfall station.
11. Finally, the boundaries of polygons around the basin perimeter are defined by drawing a perpendicular to the sides of triangles from the key points.

The AAP calculation is achieved by the application of Eq. (2.47) as already explained in detail by Şen (2008).

2.16.2.3 Isohyet Map

The word isohyet is a compound Greek word consisting of “iso” and “hyet” meaning “equal” and “rain.” Hence, collectively it implies equal rainfall lines (contour lines) similar to the equal elevation lines in a topographic map. The construction of the isohyet map is exactly the same as drawing any topographic map. The only difference is that instead of triangularization points for the topographic map, there are raingauge locations and the elevations at each of these locations are the amount of rainfall for a specific duration of time. In order to calculate the AAR from this map, the following steps are necessary:

1. Find average rainfall, R_1, between successive isohyets and this is representative of the arithmetic average for the area that is encircled by the two isohyets and the drainage boundary.
2. Find the area, A_i, on the map between the two successive isohyets.

With these two quantities (R_i and A_i), the AAR can be calculated from Eq. (2.47) similar to the previous polygon approaches.

This is the most accurate among all the previous methods, and it depends heavily on the skill of the person in drawing the isohyets. It is preferable because the map marker may know the terrain within the drainage basin and be able to adjust the isohyets to reflect natural conditions in the field. In mountainous countries, the isohyets would approximate topographic contours, since orographic rainfall usually increases by going upslope toward the mountainous areas (Sect. 2.3.1). If some measuring points show unusually heavy rainfall, then the isohyets can be clustered around such points. The advantages of the isohyet maps can be stated as follows:

1. It permits the analyst to exercise his/her own judgment and knowledge of average and specific rainfall distribution within the area.
2. It helps to fill the missing data and also adjusts suspected rainfall records.
3. There is no artificial weighting as in the polygon methods.
4. It provides opportunity to adjust the contours according to topographic features.

However, there are also disadvantages, as it is more time-consuming than most of the other methods; and it is more subjective in that the accuracy depends upon the skill of the analyst.

References

Aron, G., Wall, D. J., White, E. L., & Dunn, C. N. (1987). Regional rainfall intensity-duration-frequency curves for Pennsylvania. *Water Resources Bulletin, 23*(3), 479–485.

Bell, F.C. (1969). Generalized rainfall-duration-frequency relationships. *Journal of the Hydraulics Division, ASCE*, *95*(1), 311–327.

Benjamin, J. R., & Cornell, C. A. (1970). *Probability, statistics, and decision for civil engineers*, Dover Books on Engineering.

Bernard, M. M. (1932). Formulas for rainfall intensities of long durations. *Transactions of the ASCE, 96,* 592–624.

BOM. (1994). *Rainfall intensity Bureau of Meteorology* (2015), Accessed June 9, 2015, http://www.bom.gov.au/water/designRainfalls/ifd/index.shtml.

Burlando, P., & Rosso, R. (1996). Scaling and multiscaling models of depth-duration-frequency curves for storm precipitation. *Journal of Hydrology, 187*(1–2), 45–64.

Chen, C. I. (1983). Rainfall intensity-duration-frequency formulas. *Journal of Hydraulic Engineering, 109*(12), 1603–1621.

Chow, V. T. (1964). *Handbook of applied hydrology* (Vol. 9–49, pp. 9–62). New York: McGraw-Hill.

Chow, V. T., Maidment, D. R., & Mays, L. W. (1988). *Applied hydrology*. St. Louis, MO: McGraw-Hill Publishing Company.

Collier, C. G., & Hardaker, P. J. (1996). Estimating probable maximum precipitation using a storm model approach. *Journal of Hydrology, 183,* 277–306.

Cooke, G., & Warran, A. (1973). *Geomorphology in deserts*. London: Batsford, 394 pp.

Corrigan, P., Fenn, D. D., Kluck, D. R., & Vogel, J. L. (1999). *Probable Maximum Precipitation for California: Hydrometeorological Report No. 59*, Hydrometeorological Design Study Center, National Weather Service, National Oceanic and Atmospheric Administration, U.S. Department of Commerce, Silver Spring, MD 392 p. SGS.

Court, A. (1961). Area depth rainfall formulas. *Journal Geophysical Research, 66*(6), 1823–1831.

Desa, M. M. N., Noriah, A. B., & Rakhecha, P. R. (2001). Probable maximum precipitation for 24hr duration over Southwest Asian monsoon region—Selangor, Malaysia. *Atmospheric Research, 58,* 41–54.

Desa, M. M. N., & Rakhecha, P. R. (2007). Probable maximum precipitation for 24-h duration over an equatorial region: Part 2-Johor, Malaysia. *Atmospheric Research, 84*(1), 84–90.

Dhar, O. N., & Damte, P. P. (1969). A pilot study for estimation of probable maximum precipitation using Hershfield technique. *Indian Journal of Meteorology and Geophysics, 20* (1), 31–34.

Foufoula-Georgiou, E. (1989). A probabilistic storm transposition approach for estimating exceedance probabilities of extreme precipitation depths. *Water Resources Research, 25*(5), 799–815.

Froehlich, D. C. (1995a). Intermediate-duration-rainfall equations. *Journal of Hydrologic Engineering ASCE, 121*(10), 751–756.

Froehlich, D. C. (1995b). Long-duration-rainfall intensity equations. *Journal of Irrigation and Drainage Engineering, 121*(3), 248–252.

Froehlich, D. C. (1995c). Short-duration-rainfall intensity equations for drainage design. *Journal of Irrigation and Drainage Engineering, 121*(4), 310–311.

Garcia-Bartual, R., & Schneider, M. (2001). Estimating maximum expected short-duration rainfall intensities from extreme convective storms. *Physics and Chemistry of the Earth, Part B: Hydrology, Oceans and Atmosphere, 26*(9), 675–681.

Gumbel, E. J. (1958). *Statistics of extremes*. New York: Columbia University Press.

Hansen, E. M., Schreiner, L. C., & Miller, J. F. (1982). *Application of probable maximum precipitation estimates*. United States East of 16th meridian. Hydro-meteorological report, No. 52, 228 pp.

Hanson, C. L. (1995). Short-duration-rainfall intensity equations for drainage design. *Journal of Irrigation and Drainage Engineering, 121*(2), 219–221.

Hershfield, D. M. (1961). Estimating the probable maximum precipitation. *Journal Hydraulics Division, ASCE*, *87*(5), part 1, 99–116.

Hershfield, D. M. (1965). Method for estimating probable maximum precipitation. *Journal American Water Works Association, 57,* 965–972.

Horton, R. E. (1933). The role of infiltration in the hydrologic cycle. In *Transactions, American Geophysical Union, 14th Annual Meeting* (pp. 446–460).

Huff, F. A. (1967). Time distribution of rainfall in heavy storms. *Water Resources Research, 3,* 1007–1019.

Keers, J. F., & Wescott, P. (1977). *A computer-based model for design rainfall in the United Kingdom*. Meteorol Office Science Paper 36, London.

Koch, G. S., & Link, R. E. (1971). *Statistical analysis of geological data*, Vols I and II. New York: Dower Publications, Inc.

Koutsoyiannis, D., Kozonis, D., & Manetas, A. (1998). A mathematical framework for studying rainfall intensity-duration-frequency relationships. *Journal of Hydrology, 206,* 118–135.

Linsley, R. K. (1986). Flood estimates: How good are they? *Water Resources Research, 22*(9), 159S–164S.

Linsley, R. K., Kohler, M. A., & Paulhus, J. L. (1988). *Hydrology for Engineers* (p. 492). London: Mc-Graw-Hill Book Co.

Miller, J. F., Frederic, R. H., & Tracey, R. J. (1973). *Precipitation frequency atlas of the conterminous western United States*. NOAA Atlas 2, U.S. Department of Commerce, National

Oceanic and Atmospheric Administration, National Weather Service, Silver Springs, Maryland (Vol. 11).

Papalexiou, S. M., & Koutsoyiannis, D. (2006). A probabilistic approach to the concept of Probable Maximum Precipitation. *Advances in Geosciences, 7*(51–54), 1680–7359.

Rakhecha, P. R., & Clark, C. (2002). Areal PMP distribution for one-day to three-day duration over India. *Applied Meteorology, 9,* 399–406.

Rezacova, D., Sokol, Z., & Pesice, P. (2005). A radar-based verification of precipitation forecast for local convective storms. *Atmospheric Environment*.

Şen, Z. (1998). Average areal precipitation by percentage weighted polygon method. *Journal of Hydrologic Engineering, 3*:1(69): 69–72.

Şen, Z. (2008). *Wadi hydrology* (346 pp). New York: Taylor and Francis Group, CRC Press.

Şen, Z. (2014) *Philosophical, logical and scientific perspectives in engineering*. Berlin: Springer-Nature, 260 p.

Sherman, C. W. (1931). Frequency and intensity of excessive rainfall at Boston. *Transactions of the ASCE, 95,* 951–960.

Svensson, C., & Rakhecha, P. R. (1998). Estimation of probable maximum precipitation for dams in the Hongru River catchment, China. *Theoretical and Applied Climatology, 59,* 79–91.

Trapp, R. J., Halvorson, B. A., & Diffenbaugh, N. S. (2007). *Journal of Geophysical Research Atmosphere, 112,* D20109. doi:10.1029/2006JD008345.

U.S. Weather Bureau. (1960). *Rainfall intensity-frequency regime—Part 5: The Great Lakes Region*, Technical Paper No. 29 (TP-29), Washington, D.C. Viessman, W., Jr., Lewis, G. L., & Knapp, J. W. (1996). *Introduction to hydrology* (4th ed., p. 760). New York: Harper Collins College Publishers.

WMO. (2009). *Guidelines on analysis of extremes in a changing climate in support of informed decisions for adaptation*. By Klein Tank AMG, Zwiers FW, Zhang X. (WCDMP-72, WMO-TD/No. 1500), 56.

WMO. (2011). WMO statement on the status of the global climate in 2011 WMO-No. 1085 © World Meteorological Organization, ISBN 978-92-63-11085-5.

Yarnell, D. L. (1935). *Rainfall intensity-frequency data*. U.S. Department of Agriculture, Miscellaneous Publication No. 204, 35 pp.

Wang, B. -H. M. (1984). Estimation of probable maximum precipitation: Case studies. *Journal of Hydraulic Engineering*, *110*, 1457–1472.

http://www.springer.com/978-3-319-52355-2

Flood Modeling, Prediction and Mitigation

Şen, Z.

2018, XIV, 422 p. 213 illus., 57 illus. in color., Hardcover
ISBN: 978-3-319-52355-2